HHS Public Access

Author manuscript

Cell Rep. Author manuscript; available in PMC 2024 November 18.

Published in final edited form as:

Cell Rep. 2024 October 22; 43(10): 114829. doi:10.1016/j.celrep.2024.114829.

ERK signaling promotes resistance to TRK kinase inhibition in NTRK fusion-driven glioma mouse models

Sebastian Schmid[1,8], **Zachary R. Russell**[1,8], **Alex Shimura Yamashita**[2], **Madeline E. West**[1], **Abigail G. Parrish**[1], **Julia Walker**[1], **Dmytro Rudoy**[1], **James Z. Yan**[1], **David C. Quist**[1], **Betemariyam N. Gessesse**[1], **Neriah Alvinez**[1], **Kimberly D. Hill**[3], **Larry W. Anderson**[3], **Patrick J. Cimino**[4], **Debra K. Kumasaka**[1], **Ralph E. Parchment**[2], **Eric C. Holland**[1,5], **Frank Szulzewsky**[1,6,7,9,*]

[1]Human Biology Division, Fred Hutchinson Cancer Center, Seattle, WA 98109, USA

[2]Clinical Pharmacodynamic Biomarkers Program, Applied/Developmental Research Directorate, Frederick National Laboratory for Cancer Research, Leidos Biomedical Research, Inc., Frederick, MD 21701, USA

[3]Pharmacokinetics Laboratory, Developmental Therapeutics Program, Frederick National Laboratory for Cancer Research, Frederick, MD 21701, USA

[4]Surgical Neurology Branch, National Institute of Neurological Disorders and Stroke, National Institutes of Health, Bethesda, MD 20892, USA

[5]Seattle Translational Tumor Research Center, Fred Hutchinson Cancer Center, Seattle, WA 98109, USA

[6]Huntsman Cancer Institute, University of Utah, Salt Lake City, UT 84112, USA

[7]Department of Neurosurgery, Clinical Neurosciences Center, University of Utah, Salt Lake City, UT 84112, USA

[8]These authors contributed equally

[9]Lead contact

SUMMARY

Pediatric-type high-grade gliomas frequently harbor gene fusions involving receptor tyrosine kinase genes, including neurotrophic tyrosine kinase receptor (NTRK) fusions. Clinically, these tumors show high initial response rates to tyrosine kinase inhibition but ultimately recur

*Correspondence: frank.szulzewsky@hsc.utah.edu.

AUTHOR CONTRIBUTIONS

Conceptualization, S.S., Z.R.R., D.K.K., R.E.P., E.C.H., and F.S.; performed experiments, S.S., Z.R.R., A.S.Y., M.E.W., J.W., D.R., J.Z.Y., K.D.H., L.W.A., and F.S.; data analysis, S.S., Z.R.R., A.S.Y., A.G.P., D.C.Q., B.N.G., N.A., K.D.H., L.W.A., P.J.C., and F.S.; original manuscript writing, S.S., P.J.C., E.C.H., and F.S.; review and editing, E.C.H. and F.S.; funding acquisition, E.C.H.; supervision, R.E.P., E.C.H., and F.S. All authors read, reviewed, and approved the manuscript.

DECLARATION OF INTERESTS

The authors declare that they have no competing interests.

SUPPLEMENTAL INFORMATION

Supplemental information can be found online at https://doi.org/10.1016/j.celrep.2024.114829.

due to the accumulation of additional resistance-conferring mutations. Here, we develop a series of genetically engineered mouse models of treatment-naive and -experienced NTRK1/2/3 fusion-driven gliomas. All tested NTRK fusions are oncogenic *in vivo*. The NTRK variant, N-terminal fusion partners, and resistance-associated point mutations all influence tumor histology and aggressiveness. Additional tumor suppressor losses greatly enhance tumor aggressiveness. Treatment with TRK kinase inhibitors significantly extends the survival of NTRK fusion-driven glioma mice, but fails to fully eradicate tumors, leading to recurrence upon treatment discontinuation. Finally, we show that ERK activation promotes resistance to TRK kinase inhibition and identify MEK inhibition as a potential combination therapy. These models will be invaluable tools to study therapy resistance of NTRK fusion tumors.

Graphical abstract

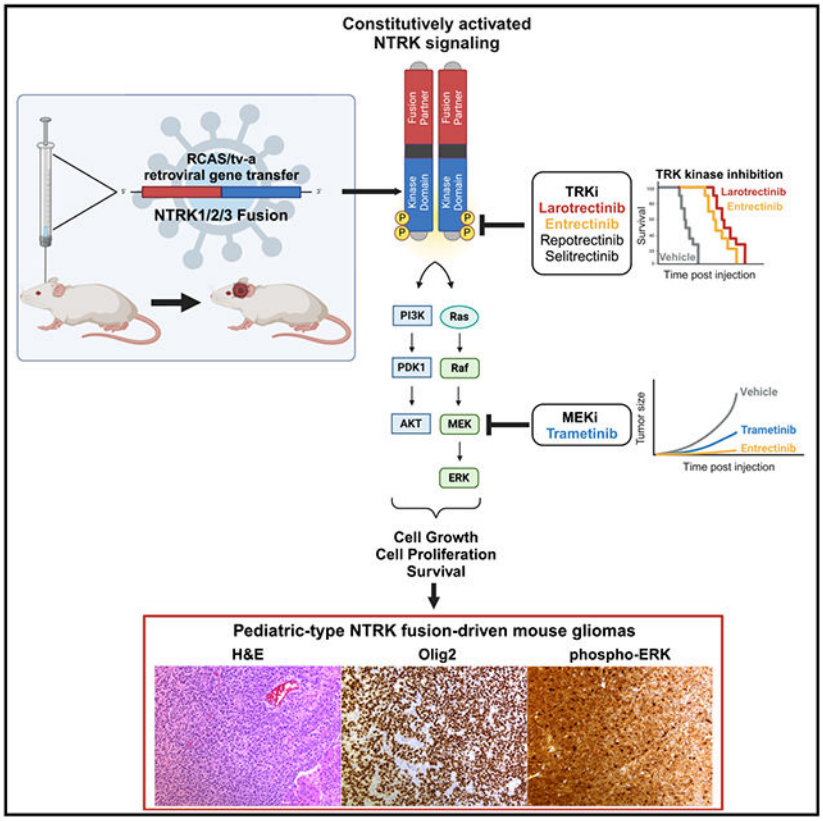

In brief

Here, Schmid et al. develop a series of NTRK fusion-driven GEMMs of pediatric-type glioma. Treatment with TRK kinase inhibitors significantly prolongs survival, but tumors eventually recur due to treatment-resistant persister cells. These tumors upregulate the Ras-Raf-MEK-ERK and PI3K-AKT-mTOR pathways, and MEK inhibition by itself leads to a significant growth inhibition.

INTRODUCTION

Gene fusions involving the three *NTRK* (neurotrophic tyrosine kinase receptor) genes are estimated to be present in up to 1% of all solid tumors and occur with a multitude of different upstream fusion partners.[1,2] Large-scale next-generation sequencing efforts have identified recurrent *NTRK* gene fusions in subsets of pediatric-type high-grade gliomas[3-5] with a prevalence ranging from 0.4% to 40%, depending on the exact tumor type.[6] In these pediatric-type tumors, the *NTRK* fusions are frequently the only known oncogenic drivers and potentially the tumor-initiating events. In addition to being found in pediatric-type gliomas, *NTRK* fusions are also found in adult-type gliomas, albeit at a lower frequency and frequently along with other common aberrations (such as gain of chromosome 7 and loss of chromosome 10), suggesting that they may not be the initiators or main oncogenic driver mutations in these tumors. Recurrent *NTRK* fusions have also been identified in a variety of peripheral cancers (including salivary gland tumors, soft-tissue sarcomas, and infantile fibrosarcoma, as well as thyroid, colon, skin, and lung cancers), in both pediatric and adult patients.[7]

Clinical trials with the first-generation TRK-specific tyrosine kinase inhibitors (TKIs) larotrectinib (LOXO-101) and entrectinib (RXDX-101) have reported high overall response rates in *NTRK* fusion-positive solid tumors, including both peripheral tumors and brain tumors (both primary and metastatic).[1,7-10] However, these responses are transient, and tumors ultimately progress due to the presence of residual persister cells that ultimately acquire additional primary mutations in the kinase domain of the *NTRK* fusion or secondary mutations in downstream pathway effectors such as Ras or Raf and eventually lead to tumor recurrence. Although novel second-generation TKIs, such as selitrectinib (LOXO-195) and repotrectinib (TPX-0005), can overcome some of these resistances, tumors frequently also become resistant to these inhibitors.[11-13] The inability of current clinical inhibitors to elicit a long-term tumor regression highlights the necessity to better understand the biology of NTRK fusions and of fusion-positive tumors, as well as the cellular responses of these tumors to tyrosine kinase inhibition *in vivo*.

Genetically engineered mouse models (GEMMs) of human cancers are valuable tools for preclinical drug testing and for studying the underlying oncogenic drivers and activated molecular pathways in these tumors.[14,15] GEMMs have several advantages over traditional patient-derived xenograft models, including the use of immune-competent mice as well as the ability to introduce specific driver mutations in a defined genetic background. We have previously used the RCAS/tv-a system (RCAS stands for replication-competent ASLV long terminal repeat [LTR] with a Splice acceptor) for somatic cell gene transfer to study the functions of common genetic drivers in glioma (such as PDGF or loss of NF1) as well as gene fusions found in meningioma or ependymoma.[16-19] This system has specific advantages over germline GEMM models, such as the ability to rapidly modify or mutate the oncogenic driver or introduce additional drivers or tumor suppressor losses.

Although the genomic landscapes differ between adult-type and pediatric-type tumors, understanding what pathways are dysregulated by strong oncogenic drivers (such as gene fusions) in pediatric-type gliomas can be used to understand the overall biology

of cancer and adult glioma. Several unanswered questions remain about the biology and oncogenic capacities of these fusions. Are these gene fusions sufficient to induce tumors experimentally *in vivo* and do the different fusions vary in their oncogenic potential? Do the different NTRK fusions respond to each TKI equally and does the therapeutic response seen in culture mimic that seen *in vivo*?

In this study, we addressed these questions by modeling eight different NTRK fusion-driven mouse gliomas using the RCAS/tv-a system. We found that all eight tested NTRK fusions were able to induce tumors when expressed in mice but observed significant differences in the oncogenic potentials of different fusions. The oncogenesis was significantly enhanced when introducing additional tumor suppressor losses, most importantly *Cdkn2a* loss. We then determined the therapeutic responses of *NTRK* fusion-driven cell-line models to TKIs *in vitro* and subsequently performed preclinical *in vivo* trials, treating mice harboring *NTRK* fusion-driven gliomas with the two first-generation TKIs larotrectinib and entrectinib. *In vivo,* we observed significantly increased survival rates for all fusion tumor types; however, all tumors ultimately recurred after treatment discontinuation due to the presence of treatment-resistant persister cells. Finally, we identify MEK inhibition as a potential combination therapy. In summary, our results suggest that *NTRK* gene fusions are strong oncogenic drivers and the likely tumor-initiating events in pediatric-type *NTRK* fusion-positive gliomas. Tyrosine kinase inhibition is able to significantly extend survival; however, it ultimately failed to completely eliminate tumors, eventually resulting in tumor recurrence.

RESULTS

Expression of NTRK1/2/3 fusions alone is sufficient for the formation of gliomas in mice

To determine if the expression of different *NTRK1/2/3* gene fusions is sufficient to induce the formation of glioma-like tumors in mice, we cloned the human coding sequences of eight *NTRK* fusions frequently found in human pediatric-type high-grade gliomas into the RCAS retroviral vector, including two *NTRK1* fusions (*TPM3-NTRK1* [*TN1*], *CHTOP-NTRK1* [*CN1*]), three *NTRK2* fusions (*GKAP1-NTRK2* [*GN2*], *NACC2-NTRK2* [*NN2*], and *QKI-NTRK2* [*QN2*]), and three *NTRK3* fusions (*ETV6-NTRK3* [*ETV6-N3*], *EML4-NTRK3* [*EML4-N3*], and *BTBD1-NTRK3* [*BN3*]) (Figures S1A and S1B).

We used the RCAS/tv-a system for somatic cell gene transfer in combination with Nestin/tv-a (N/tv-a) mice[15] to intracranially express the different *NTRK* fusion constructs in Nestin-positive stem and progenitor cells. While *NTRK* gene fusions are enriched in infantile/pediatric patients,[3-5] they are also found in adult patients[20,21]; we therefore intracranially expressed the different *NTRK* fusion constructs in mice of different ages (postnatal day 0–2 [p0–p2], 1-week-old mice (p7), and 5- to 7-week-old adult mice).

Each of the analyzed *NTRK* gene fusions was able to induce the formation of tumors from Nestin-expressing cells in the brain on their own without the loss of additional tumor suppressors (Figure S1C). We observed prominent differences in tumor penetrance and aggressiveness depending on the age of transgene expression (Figures 1A-1C and S1C-S1F). Tumors induced in p0–p2 mice were frequently of high penetrance and generally more aggressive, whereas tumors induced in 1-week-old mice displayed a high

penetrance but were generally slow growing and remained non-symptomatic even 120 days postinjection (study endpoint). In rare instances when tumors grew to a larger size and became symptomatic, these were usually centered around the third ventricle (Figure S1G), suggesting that Nestin-positive cells in that area are more susceptible to oncogenic transformation by *NTRK* fusions compared to cells near the lateral ventricles at that point in development. Of note, *NTRK* gene fusions have been observed in human pediatric diffuse midline gliomas.[21] Upon expression in adult *Cdkn2a* wild-type mice, only *CHTOP-NTRK1* was able to induce the formation of small non-symptomatic tumors (two of three mice), whereas the other tested *NTRK* fusions failed to do so. In these adult *Cdkn2a* wild-type tumors, only a minority of cells in the tumor stained positive for the TRK fusion kinase domain.

Taken together, our data suggest that expression of *NTRK* fusions alone is sufficient to induce tumor formation without the loss of additional tumor suppressor and that these fusions are the likely tumor-initiating events in *NTRK* fusion-positive pediatric-type high-grade gliomas. The age of transgene expression has a significant influence on the aggressiveness of the resulting tumors.

Additional loss of tumor suppressors (*Cdkn2a* and *Pten*) increases aggressiveness of *NTRK* fusion-driven gliomas

Deletions in *CDKN2A/B* have been reported in 12%–25% of *NTRK1/2/3* fusion-positive pediatric-type high-grade gliomas[3-5]; inactivating mutations in *PTEN* have been reported in at least one *NTRK1/2/3* fusion-positive pediatric-type high-grade glioma.[3] To assess if the loss of *Cdkn2a* affects the growth behavior of *NTRK* fusion-driven gliomas in our system, we intracranially expressed the different *NTRK* fusions in Nestin-positive cells of N/tv-a *Cdkn2a* null mice. In addition, we intracranially co-expressed *TN1* and *CN1* in combination with a short hairpin against *Pten*[17] in N/tv-a *Cdkn2a* wild-type mice to model *Pten* loss.

Loss of *Cdkn2a* significantly enhanced tumor growth and increased tumor histologic grade (Figures 1D, 1E, and S1H-S1K). The age at initial transgene expression significantly impacted tumor latency. Mice with tumors induced at p0 frequently became symptomatic before 21 days of age; however, the tumors also caused hydrocephalus formation in a large percentage of mice, whereas tumors induced in adult mice showed a significantly longer latency compared to either p0 or p7 tumors. Adult-initiated tumors—regardless of the gene fusion—frequently developed an extra-axial and extracranial component in addition to the intraparenchymal tumor component.

We observed significant differences in the latency of *Cdkn2a* null tumors derived from different *NTRK* fusions, in part even if they were derived from the same *NTRK1/2/3* variant (Figures 1D and S1H-S1I). Tumors induced by *TN1, CN1, GN2, EML4-N3,* or *BN3* generally showed the lowest latency (17–21 and 26–28 days median survival for p7 and adult tumors, respectively), followed by either *QN2* or *NN2* (23–24 and 41–42 days median survival for p7 and adult tumors, respectively), whereas tumors induced by *ETV6-N3* displayed the longest latency (38 and 53 days median survival for p7 and adult tumors, respectively). The *ETV6-N3* fusion sequence reported from glioma samples contains a breakpoint that generates a shorter kinase domain sequence compared to the other two

NTRK3 fusions in our cohort (Figures S1A and S1B). A variant of *ETV6-N3* with a longer kinase domain sequence—equal to *EML4-N3* and BN3—has been reported in other cancers (Figure S1A and S1B).[22] Expression of this longer variant led to a non-significant trend ($p = 0.09$) toward longer latency (55 days versus 38 days median survival) (Figure S1L). These results suggest that the longer latency of tumors induced by *ETV6-N3* compared to tumors induced by *EML4-N3* or *BN3* is not caused by the truncated *NTRK3* kinase domain present in *ETV6-N3*.

All analyzed tumors involved supratentorial structures (cerebral hemisphere, hippocampus, thalamus, or striatum). A large number involved the cerebral hemispheres (cerebral cortex and/or subcortical white matter). A small number of supratentorial tumors were not observed in the cerebrum but instead were intraventricular (lateral ventricles) or were found deeper, to involve the thalamus and striatum. Tumors involving the cerebral hemispheres frequently also invaded deeper structures (hippocampus, thalamus, and/or striatum). None of the tumors involved infratentorial structures (brain stem or cerebellum) or the spinal cord. The overall neuroanatomical localization of these mouse fusion tumors, mainly involving the cerebral hemispheres, is inline with human NTRK-fusion gliomas, particularly the infant-type hemispheric glioma.

The majority of the *NTRK* gene-fusion-driven tumors (*TN1, CN1, GN2,* adult *NN2, ETV6-N3,* and pediatric *QN2*) appeared histologically as diffuse astrocytic gliomas, demonstrating an infiltrating growth pattern, and were of glial origin (Figures 1E, S1J-S1K, and S1M). In general, these gliomas had variable mitotic activity and occasionally showed palisading necrosis. The astrocytic-appearing neoplastic cells in these tumors were characterized by enlarged, angulated, and hyperchromatic nuclei present on a fibrillary background. A couple of the *NTRK* fusion tumors (*EML4-N3* and pediatric *NN2*) appeared to have a more compact arrangement, with the cells appearing more epithelioid, characterized by round cells with more defined cell borders, abundant eosinophilic cytoplasm, and variably enlarged and round nuclei with prominent nucleoli. One of the *NTRK* gene fusion tumors (adult *QN2*) had a predominantly spindled cell component, which was almost sarcomatous-like, and the cells had a compact fascicular arrangement.

Loss of *Pten* expression had a more subtle impact on tumor growth compared to *Cdkn2a* loss (Figures 1F, S1D, S1N, and S1O). There was no significant difference in the survival of *TN1* or *CN1* tumors upon loss of *Pten* expression; however, a subset of tumors originating from the lateral ventricles were of larger size and became symptomatic. Histologically, these tumors often demonstrated oligodendroglial-like perinuclear clearing, which differed from that of *Pten* wild-type or *Cdkn2a* null tumors.[23]

As described above, adult-initiated tumors frequently consisted of an intraparenchymal and a connected extraparenchymal component. The extraparenchymal component frequently grew as an extra-axial tumor and also grew out through the needle tract as extracranial tumor tissue. Similar to the intraparenchymal tumor component, tumor cells in the extraparenchymal tumors were also Olig2 positive, indicating a glial tumor lineage (Figure S1P). Magnetic resonance imaging (MRI) (T1 weighted and T2 weighted, pre- and postcontrast) on mice harboring intracranial *TPM3-NTRK1* tumors that exhibited

extracranial tumor growth showed that the extracranial and, to a lesser degree, the extra-axial tumor components were contrast enhancing, whereas the intraparenchymal tumor component was not. This suggests that the extracranial and extra-axial tumor components are more permeable to the contrast agent and therefore potentially also to small-molecule inhibitors (Figure S1Q).

Since *NTRK* gene fusions are also found in non-CNS cancers (including lung, liver, and colon cancers), we also expressed these gene fusions in the flank and abdominal cavity of N/tv-a *Cdkn2a* null mice and observed the formation of highly aggressive sarcomatous-like spindle cell neoplasms that appeared to have arisen from the soft tissue and encased nearby organs such as colon and kidney (Figures S1R-S1U).

Taken together, these results suggest that additional loss of tumor suppressors substantially increases the aggressiveness of *NTRK* fusion-driven gliomas. The N-terminal fusion partners can influence tumor aggressiveness and latency.

Modeling of *NTRK* fusion-driven mouse gliomas harboring resistance-associated kinase domain point-mutant variants

Targeted sequencing of recurrent patient tumors has recurrently identified point mutations in the kinase domain of *NTRK* gene fusions, suggesting that these mutations may constitute an early escape mechanism for *NTRK* fusion-positive tumor cells to bypass TKIs.[7] The most common mutation hotspots include the gatekeeper residue (F589L in NTRK1), the solvent front residue (G595R in NTRK1), and xDFG mutations in the activation loop (G667C in NTRK1). The gatekeeper and the solvent front mutations are also frequently observed in combination.[2,7]

To assess if these kinase domain mutations influence tumor latency, we intracranially expressed the different *TPM3-NTRK1* kinase point-mutant variants in 1-week-old N/tv-a *Cdkn2a* null and wild-type mice (Figures S1V-S1Z). Similar to unmutated TPM3-NTRK1, all four mutant variants were able to rapidly induce tumor formation in *Cdkn2a* null mice (Figures S1X and S1Y). The F589L, G595R, and F589L-G595R mutant variants displayed a latency similar to that of unmutated TPM3-NTRK1, whereas the G667C mutant version displayed a significantly longer latency (27 days versus 21 days, $p = 0.0048$).

In N/tv-a *Cdkn2a* wild-type mice, the F589L, G595R, and G667C mutant variants displayed a similar oncogenic potential compared to unmutated TPM3-NTRK1, with a high tumor penetrance, but tumors generally remained small and non-symptomatic even 120 days postinjection (Figures S1V and S1W), apart from a small number of symptomatic tumors originating from the third ventricle. By contrast, tumors induced by the expression of TPM3-NTRK1-F589L-G595R were significantly faster growing compared to tumors induced by unmutated TPM3-NTRK1 ($p = 0.026$), although the majority of tumors still remained non-symptomatic 120 days after induction. In addition, we observed the formation of large symptomatic tumors originating from the lateral ventricles in 2 of 14 mice injected with TPM3-NTRK1-F589L-G595R (Figure S1Z), something not observed upon expression of any of the other constructs.

Taken together, our data suggest that by expressing *NTRK* fusion variants that harbor resistance-associated kinase point mutations, we can induce the formation of gliomas that mimic treatment-experienced tumors. Some of these kinase point mutations influence tumor aggressiveness.

NTRK fusion-induced mouse gliomas show activation of the PI3K-AKT-S6 and RAF-MEK-ERK pathways

To characterize these mouse gliomas in more detail, we performed immunohistochemistry (IHC) stainings for the TRK kinase domain and the glial markers Olig2 and GFAP, as well as the proliferative marker Ki67 (Figures 2 and S2A-S2H). Tumors derived from *TN1, CN1, GN2, NN2,* or *ETV6-N3* were uniformly positive for the glial marker Olig2 regardless of the age of injection, whereas tumor cells frequently also stained positive for GFAP in pediatric but not in adult tumors. Tumors derived from *QN2, EML4-N3,* or *BN3* fusions predominantly stained negative for GFAP (both pediatric and adult), and only a subset of tumor cells stained positive for Olig2. All tumors showed a high abundance of Ki67-positive cells.

Two of the main mitogenic downstream pathways activated by receptor tyrosine kinases, including NTRK receptors, are the PI3K-AKT-S6 and RAF-MEK-ERK pathways. To analyze if these pathways are also activated in the different NTRK fusion-driven mouse gliomas, we performed IHC stainings for phospho-ERK, phospho-AKT, and phospho-S6 and observed robust staining for all three epitopes in the different tumors, suggesting that both the PI3K-AKT-S6 and the RAF-MEK-ERK pathway are activated in these tumors (Figures 2 and S2A-S2H).

Taken together, our results indicate that *NTRK* fusion-driven mouse tumors are of glial lineage and activate both the PI3K-AKT-S6 and the RAF-MEK-ERK pathway.

Development of *NTRK* fusion cell-line-based models to test the efficacy of various TKIs against resistant-associated kinase point mutations *in vitro*

To assess the efficacy of TKI treatment against *NTRK* fusion-driven cells *in vitro,* we established several *NTRK* fusion-driven cell-line models. We first transduced NIH-3T3-tv-a cells with RCAS viruses encoding GFP, TN1, GN2, or ETV6-N3 and subsequently performed 3D spheroid growth assays (Figures 3A, S3A, and S3B). In the absence of a strong oncogenic driver, NIH 3T3 cells are unable to grow in 3D spheroid conditions, whereas oncogenic signaling can induce the growth of these cell spheroids.[18,19,24] While GFP-expressing cells did not grow as spheroids, spheroids derived from *NTRK* gene-fusion-expressing cells continued to grow in size over several days (Figures 3B and S3C). We tested the efficacy of four different TKIs—larotrectinib, entrectinib, and the two second-generation inhibitors, repotrectinib (TPX-0005) and selitrectinib (LOXO-195)—to inhibit the growth of these spheroids (Figures 3C-3E and S3C-S3E). Treatment with any of the four TKIs did not influence the growth of GFP-expressing spheroids, whereas the growth of *NTRK* fusion-driven spheroids was inhibited by all four TKIs in a dose-dependent manner. Entrectinib treatment was more effective in *TN1*-expressing cells compared to cells expressing *GN2*

or *ETV6-N3,* but there was otherwise no difference in the efficacy of the different TKIs between the different *NTRK* fusions (Figure S3E).

Resistance to therapy against first-generation TKIs frequently occurs via the accumulation of *NTRK* kinase domain point mutations. To analyze how the different point mutations influence treatment response *in vitro,* we transduced NIH-3T3-tv-a cells with RCAS viruses encoding the different TPM3-NTRK1 mutants (F589L, G595R, G667C, and F589L-G595R) and tested the efficacy of the different TKIs to inhibit the growth of these spheroids (Figures 3F-3M, S3B, and S3F-S3J). Cells expressing the F589L gatekeeper residue mutation were resistant to larotrectinib but still susceptible to entrectinib, repotrectinib, and selitrectinib (Figures 3F and S3J), whereas the G595R solvent front mutation conferred resistance to both larotrectinib and entrectinib (Figures 3J and S3J). Cells expressing either the G667C xDFG mutation or a combination of the F589L and G595R mutations were completely resistant to selitrectinib and showed a decreased sensitivity to repotrectinib (Figures S3F-G, and S3J). Western blots of TKI-treated cells showed a decrease in p-TRK, p-ERK, and p-AKT levels that reflected the susceptibilities of the different resistance point mutations to the different TKIs (Figures 3E-3I, 3M, and S3F-G).

We then established cell lines from primary mouse flank tumors induced by the injection of RCAS viruses encoding TPM3-NTRK1-F589L, TPM3-NTRK1-G595R, or TPM3-NTRK1-F589L-G595R into N/tv-a *Cdkn2a* null mice and performed 3D spheroid assays with these cells. We again observed that TKI treatment was able to inhibit the growth of these spheroids in a resistance-mutation-dependent manner that mirrored our findings from the NIH-3T3-tv-a cell-line models (Figures 3G, 3K, and S3H-S3I).

Taken together, the results show that *NTRK* fusion-driven cell-line models can predict the response of different kinase point mutants to first- and second-generation TKIs.

Resistance-associated kinase domain point mutations influence the response of *NTRK* fusion-driven cells to TKI treatment *in vivo*

To evaluate if the different TKIs can induce the regression of intracranial *NTRK* fusion-driven gliomas *in vivo,* we expressed *EML4-N3* in N/tv-a *Cdkn2a* null mice and treated these mice 17 days after tumor induction (upon occurrence of first tumor-related symptoms) with either vehicle (four mice) or larotrectinib (100 mg/kg), entrectinib (60 mg/kg), repotrectinib (20 mg/kg), or selitrectinib (20 mg/kg) (three mice per TKI group) twice a day (b.i.d.) for 25 h (three injections in total). Mice were euthanized 1 h after the third treatment and brains were formalin fixed and subsequently analyzed by IHC for markers of apoptosis (cleaved caspase 3 [CC3]) and proliferation (phospho-histone H3 [pHH3] and Ki67) as well as p-ERK and p-S6.

All four TKIs were able to reduce the levels of p-S6 and p-ERK staining in the tumor tissues (Figure 4A). Treatment with either entrectinib or repotrectinib (2.86% and 3.36% CC3-positive cells in the tumor tissue, respectively) or, to a lesser degree, selitrectinib (1.07%) significantly increased the number of CC3-positive cells compared to vehicle-treated mice (0.45%), whereas larotrectinib did not (0.66%) (Figure 4B). By contrast, only treatment with larotrectinib (1.51% pHH3- and 5.73% Ki67-positive cells) led to a

reduction in proliferating cells compared to vehicle-treated mice (6.42% pHH3- and 14.18% Ki67-positive cells) (Figures 4B and S4A). While we observed a decrease in overall p-S6 and p-ERK staining, a small subset of tumor cells still showed ERK/S6 activation (Figures S4B and S4C), suggesting that these cells may be less affected by TKI treatment. Especially in entrectinib-treated mice, we observed higher residual levels of p-ERK and p-S6 staining in tumor cells at the invasive front (Figures S4B and S4C).

We then performed TKI treatments in mice harboring intracranial gliomas driven by EML4-N3-G623R, which harbors a point mutation in the solvent front residue of the NTRK3 kinase domain (analogous to the G595R mutation of NTRK1). Mice were again treated 17 days after tumor induction for 25 h with either vehicle (five mice) or the four TKIs (same concentrations as before, four mice per TKI group).

Treatment with either of the two first-generation TKIs did not reduce the levels of p-S6 or p-ERK staining in EML4-N3-G623R tumors compared to vehicle-treated mice (Figure 4C), nor was larotrectinib able to induce a reduction in the number of pHH3-positive cells (2.42% versus 3.16% in larotrectinib- and vehicle-treated mice, respectively) or Ki67-positive cells (17.21% versus 25.29% in larotrectinib- and vehicle-treated mice, respectively) (Figures 4D and S4D). Similarly, entrectinib treatment was unable to increase CC3 staining (0.52% versus 0.49% CC3-positive cells in entrectinib- and vehicle-treated mice, respectively) (Figures 4C and 4D). By contrast, treatment with either repotrectinib or selitrectinib was able to reduce the levels of both p-ERK and p-S6 in the tumor bulk tissue; however, especially in tumor cells of the invasive edge, p-ERK and p-S6 levels remained high, suggesting that these cells are somewhat protected from or resistant to the effects of TKIs (Figures 4C and S4E). The ability of repotrectinib to induce apoptosis was significantly reduced in EML4-N3-G623R tumors, although still significant compared to vehicle-treated mice (1.04% versus 0.49% CC3-positive cells in repotrectinib- and vehicle-treated mice, respectively). Selitrectinib treatment displayed a similar ability to induce CC3 staining compared to unmutated EML4-N3 tumors (1.36% CC3-positive cells).

Taken together, our results suggest that TKI treatment can induce the regression of *NTRK* fusion-driven mouse gliomas *in vivo* within hours of treatment and that resistance-associated kinase domain point mutations can significantly influence treatment responses *in vivo*.

TKI treatment significantly prolongs the survival of *NTRK* gene fusion-driven mouse gliomas, but tumors ultimately recur after treatment discontinuation

To assess if the two first-generation TKIs, larotrectinib and entrectinib, can prolong the survival of *NTRK* fusion-driven mouse gliomas *in vivo* and if there is a difference in the response between tumors induced by different *NTRK* fusions, we selected six *NTRK* fusions and intracranially induced gliomas by RCAS viral injection into either p7 (*ETV6-N3* and *EML4-N3*) or adult (*TN1, CN1, GN2,* and *NN2*) N/tv-a *Cdkn2a* null mice and performed preclinical *in vivo* trials. To assess the initial tumor size before treatment and ensure a distribution of similarly sized tumors into each treatment group, a first T2w MRI was performed 15–25 days post tumor induction (depending on the *NTRK* fusion, see STAR Methods), and the mice were then treated with vehicle (DMSO), larotrectinib (100 mg/kg), or entrectinib (30 mg/kg) for 14 days (for dosing and toxicity experiments see

STAR Methods). The day after the last treatment, the mice received a second T2w MRI and were subsequently observed for the onset of tumor-related symptoms. No MRIs were performed for *EML4-N3* mice, since these were too young at treatment start due to the aggressive growth of these tumors.

Treatment with either larotrectinib or entrectinib significantly extended survival compared to vehicle treatment; however, treated tumors ultimately recurred upon treatment discontinuation in all mice due to the presence of residual disease and treatment-resistant persister cells (Figures 5A and S5A). The extent to which survival was prolonged differed between the different *NTRK* fusions and the two TKIs (Figure S5B). The largest increase in survival was observed for *EML4-N3*-driven tumors treated with larotrectinib (36 versus 16 days [vehicle] median survival, $p < 0.0001$) and *ETV6-N3*-driven tumors (57 [larotrectinib] and 53 [entrectinib] versus 41.5 days [vehicle] median survival, $p < 0.0001$ and $p = 0.0001$, respectively). We observed that for some fusion-driven tumor types, a specific TKI was more effective. In *CN1*-driven tumors, entrectinib treatment led to a significant survival benefit over larotrectinib treatment (48 versus 41 days median survival, respectively, $p = 0.0003$), whereas in *NN2*- (56 versus 50 days median survival, respectively, $p = 0.001$), *ETV6-N3*- (57 versus 53 days median survival, respectively, $p = 0.05$), and *EML4-N3*-driven tumors (36 versus 19 days median survival, respectively, $p < 0.0001$), larotrectinib treatment led to a significantly better outcome compared to entrectinib treatment. There was no significant difference between the two TKIs at the tested concentrations for *TN1* and *GN2* fusion-driven tumors.

We calculated the fold-change increase in tumor size based on pre- and posttreatment MRIs and observed that intraparenchymal tumors were less susceptible to TKI treatment than extraparenchymal tumors (Figure 5B). Extraparenchymal (extra-axial and extracranial) tumors were almost uniformly present in vehicle-treated mice but frequently absent or smaller in TKI-treated mice (Figures S5C and S5D). Intracranial tumors in larotrectinib- and entrectinib-treated mice were significantly smaller compared to those in vehicle-treated mice for each of the *NTRK1/2/3* fusion-driven glioma models at the end of treatment (Figures 5B and 5C). However, adult intracranial tumors (*TN1, CN1, GN2,* and *NN2*) continued to grow while on treatment with larotrectinib and entrectinib and were between 3- and 6-fold larger compared to before treatment, albeit at a lower rate compared to vehicle-treated tumors (10- to 22-fold larger compared to before treatment, depending on the tumor type). By contrast, pediatric *ETV6-N3* tumors remained stable or even shrank during TKI treatment; larotrectinib and entrectinib treatment resulted in a regression or stagnation of intraparenchymal tumor growth (66% and 100% average tumor volume, respectively, relative to before treatment start), whereas vehicle-treated tumors grew significantly (651% average tumor volume relative to the first MRI) (Figures 5D and S5E). Interestingly, the differences in survival between larotrectinib and entrectinib (such as for *CHTOP-NTRK1*) were not reflected by significantly different tumor sizes as measured by MRI.

As described above, we observed that, similar to human *NTRK* fusion-positive tumors, TKI treatment led to tumor regression/stable disease or at least reduced tumor growth in our mouse models but was unable to completely eradicate tumors, ultimately resulting in tumor recurrence once treatment was discontinued. Therefore, we sought to assess if an increased

TKI dose would be sufficient to completely ablate all tumor cells *in vivo*. To this end, we treated *TN1, CN1,* and *GN2* tumor mice with 60 mg/kg entrectinib b.i.d. ($n = 2$ per group) or vehicle for 7 days. We had previously used a concentration of 30 mg/kg b.i.d. for the 14-day treatment since higher entrectinib doses resulted in increased toxicity over longer treatment periods. While tumors in entrectinib-treated mice were significantly smaller compared to vehicle-treated tumors, treatment-resistant persister cells were present even at this increased dose, suggesting that TKI treatment alone is unable to completely eradicate these tumors *in vivo* (Figures 5E and S5F).

Our data suggest that the extracranial tumors respond significantly better to TKI treatment compared to intraparenchymal tumors. Since we observed that extracranial tumors are contrast enhancing, whereas intracranial tumors are not (Figure S1M), we speculated that increased drug influx into the tissue of extracranial tumors might contribute to the increased response. To this end, we treated five tumor-bearing mice (one *CN1,* two *GN2,* one *NN2,* and one *ETV6-N3*) for 48 h with 100 mg/kg larotrectinib b.i.d. (five treatments in total) and isolated intra- and extracranial tumor tissue, as well as hindlimb muscle and liver tissue. Mass spectrometry analysis showed that the average larotrectinib concentration in the intraparenchymal tumor tissue (0.037 ± 0.0098 ng/mg) was around 20-fold lower compared to that in the extracranial tumor tissue (0.73 ± 0.25 ng/mg; $p = 0.009$) (Figures 5F, S5G, and S5H). No significant difference was detected between extracranial tumor tissue and muscle tissue (0.76 ± 0.35 ng/mg; $p = 0.99$). These data suggest that the increased effectiveness of TKIs against extracranial tumors might in part be owed to the increased ability of these compounds to permeate into the extracranial tumor tissue.

Taken together, our results show that treatment with larotrectinib and entrectinib can significantly prolong the survival of *NTRK* fusion-driven mouse gliomas *in vivo*; however, ultimately, all tumors recurred upon treatment discontinuation due to the presence of persister cells. Tumors derived from different *NTRK* fusions do not respond equally to the two TKIs.

MEK inhibition shows efficacy in NTRK fusion-driven mouse tumors

To investigate why treatment with entrectinib was frequently less effective compared to larotrectinib, we treated several mice harboring *ETV6-N3, TN1,* or *CN1* gliomas for 14 days with either larotrectinib (100 mg/kg) or entrectinib (30 mg/kg) b.i.d. and euthanized them 1 h after the last treatment. Treatment with either larotrectinib or entrectinib led to a similar decrease in p-AKT levels in tumor tissues compared to vehicle treatment. However, p-ERK levels were considerably higher in tumor tissues of mice treated with entrectinib compared to larotrectinib, albeit lower than in vehicle-treated mice (Figures 6A and S6A). This is in line with our results from the 25-h short-term treatments, in which entrectinib also resulted in elevated residual p-ERK levels (Figures S4A and S4B).

Since we observed increased p-ERK levels in tumors that tended to display a shorter survival, we speculated that ERK signaling plays a critical role in *NTRK* fusion-driven tumors. To test the efficacy of downstream pathway inhibition of both the PI3K-AKT-S6 and the RAF-MEK-ERK pathways, we treated our previously established cell-line models (*in vitro*-transduced NIH 3T3 cells and primary mouse tumor cells) with repotrectinib (TKI),

trametinib (MEKi), taselisib (PI3Ki), or PLX3894 (BRAFi) and performed 3D spheroid assays. While BRAF inhibition had no effect, inhibition of both PI3K and MEK was able to inhibit the growth of NTRK fusion-driven cells (Figures 6B and 6C). Finally, combination treatment with TKIs and MEK inhibitors led to a more pronounced growth inhibition than either alone (Figures 6B and 6C). TKI treatment decreased p-AKT levels but only partially reduced p-ERK levels, whereas MEK inhibition effectively reduced p-ERK levels but led to an increase in p-AKT levels. Combination treatment with TKIs and MEK inhibitors led to a decrease in both p-AKT and p-ERK levels (Figures 6D and S6B).

We then decided to test the efficacy of MEK inhibition *in vivo*. Given the poor penetration of these inhibitors into the brain, for the mechanistic question of downstream dependencies, we induced ETV6-N3-driven tumors in the flank of p7 N/tv-a *Cdkn2a* null mice (Figure S1O). Mice with palpable tumors were treated with vehicle ($n = 11$), trametinib (1 mg/kg, $n = 12$), or entrectinib (15 mg/kg, $n = 5$) for 5 weeks. Tumor calipers were measured daily. We observed that treatment with trametinib significantly inhibited the growth of tumors (Figures 6E and S6C). However, whereas entrectinib treatment resulted in the stabilization or even regression of tumors, trametinib-treated tumors continued to grow while on treatment, albeit to a significantly lower degree compared to vehicle-treated tumors. These data suggest that RAF-MEK-ERK signaling contributes to the growth of *NTRK* fusion-driven tumors *in vivo*.

Taken together, these results highlight the importance of the RAF-MEK-ERK signaling pathway in NTRK fusion-driven tumors. *In vivo,* MEK inhibition by itself was able to slow the growth of *NTRK* fusion-driven tumors, albeit less effectively compared to TKIs. *In vitro,* a combination of TKI and MEK inhibition is superior to either treatment alone.

DISCUSSION

Most adult IDH (isocitrate dehydrogenase)-wild-type glioblastomas harbor a highly aberrant genome, leading to multiple concurrent and redundant drivers that make targeting of specific pathways difficult. By contrast, pediatric-type high-grade gliomas are enriched for gene fusions involving receptor tyrosine kinase genes (such as *NTRK1-3, ALK,* and *ROS1*) and harbor an otherwise relatively stable genome, making them ideal candidates for targeted therapy with TKIs. These inhibitors show high initial response rates, frequently leading to either tumor regression or stable disease; however, surviving therapy-resistant persister cells eventually accumulate additional mutations, allowing them to regrow the tumor even in the presence of the kinase inhibitors.[1,25] The blood-brain barrier limits drug availability in the brain and brain tumors, further impeding the efficacy of these inhibitors.

Using the RCAS/tv-a system,[15] we have developed a series of novel GEMMs of pediatric-type *NTRK* fusion gene-driven high-grade gliomas. These GEMMs have several advantages over conventional xenograft or syngraft/allograft models and even over germline GEMMs. Our RCAS/tv-a tumor models are caused by somatic cell gene transfer of defined oncogenes (such as *NTRK* gene fusions) into *Nestin*-expressing neural stem and progenitor cells. Since these tumors arise *de novo* from within the mouse's own cells, there is no potential graft-versus-host effect that might occur in allograft models, and in contrast to xenograft transplantation models, these tumors can be induced in mice that harbor a completely intact

immune system. An advantage over germline GEMMs is the flexibility of this system, which allows us to rapidly introduce additional mutations into the system to model, for example, treatment-experienced tumors, such as resistance-associated point mutations in the fusion protein kinase domain, and test different *NTRK* fusion types. These models will help us to better understand the biology of treatment response and resistance to therapy of *NTRK* fusion-driven pediatric-type gliomas in a genetically defined system with tumors that are caused and driven by the actual *NTRK* gene fusion and that therefore directly rely on its activity.

All tested *NTRK* fusions were highly oncogenic when expressed in the brain and, in the absence of *Cdkn2a* expression, resulted in uniform tumors that are ideal model systems for preclinical *in vivo* trials. Our data suggest that *NTRK* gene fusions indeed could be the initiating events in humans and are consistent with the relative lack of additional genetic rearrangement found in these tumors relative to adult gliomas. We also found that tumors were more aggressive when induced in younger mice (e.g., shortly after birth) compared to older mice, which may give an explanation of why these gene fusions are enriched in tumors in infants and younger children.

There is a plethora of different *NTRK* fusions and clinical trials (with either *NTRK* fusion-positive brain or peripheral tumors) that show that not all tumors respond to TKI treatment equally, sometimes even if they harbor the same gene fusion.[1,7,8] This might be in part due to the presence of additional oncogenic driver mutations or the presence of kinase domain point mutations, but it is also unclear if different *NTRK* fusions (and the tumors that harbor these fusions) are equally susceptible to TKI treatment. All of these individual fusions are rare in humans, making trials comparing drugs against tumors with specific fusions impractical. Therefore, mouse models with a defined genetic background of tumors driven by specific gene fusions and their resistant mutations are needed.

Tumors induced by different NTRK fusions varied significantly in aggressiveness. Tumors induced by *EML4-NTRK3, BTBD1-NTRK3, CHTOP-NTRK1, TPM3-NTRK1*, and *GKAP1-NTRK2* were generally the most aggressive, whereas tumors induced by *ETV6-NTRK3* displayed the longest latency. This is especially noteworthy, since (1) *ETV6-NTRK3, EML4-NTRK3,* and *BTBD1-NTRK3* all harbor the same NTRK3 kinase domain and (2) *ETV6-NTRK3* is one of the most common *NTRK* fusions in pediatric-type gliomas and other peripheral tumors.[3,4,7] It remains unclear why *ETV6-NTRK3* is less oncogenic compared to the other fusions, and it might be speculated that the N-terminal fusion partner can influence the oncogenicity of the *NTRK* fusion, potentially through varying abilities to induce fusion dimerization necessary for autophosphorylation and activation.[26]

All tested *NTRK* fusion-driven mouse gliomas responded to treatment with the two first-generation TKIs, larotrectinib and entrectinib. We observed treatment responses within the first 25 h of treatment, accompanied by the downregulation of oncogenic PI3K-AKT-S6 and RAF-MEK-ERK signaling pathways in a majority of cells. Similar to *NTRK*fusion-positive tumors in patients, tumor clearing was incomplete, and surviving persister cells led to the regrowth of tumors after treatment discontinuation. The adult-induced tumors even continued to grow while on treatment, albeit at a slower rate than vehicle-treated

tumors. Limited drug penetration into the brain of the two first-generation inhibitors likely contributed to the incomplete responses of intraparenchymal brain tumors, since extracranial and extra-axial tumors showed a more complete response. Mass spectrometry data showed that the concentration of larotrectinib in the tumor tissue was 20-fold lower in intraparenchymal tumors compared to extracranial tumors. These data highlight the necessity for improved drug-delivery methods to overcome the blood brain barrier. However, extracranial and extra-axial tumors also regrew in some cases, suggesting that persister cells were also able to survive higher TKI concentrations. Future characterization of these treatment-resistant persister cells will be necessary and important in order to develop effective combination therapies to improve the efficacy of TKIs.

We observed reproducible differences in the therapeutic responses to TKIs between the various *NTRK* gene fusion-driven tumors at the tested inhibitor concentrations. *CHTOP-NTRK1*-driven tumors responded significantly better to entrectinib over larotrectinib treatment, while in *NACC2-NTRK2-, ETV6-NTRK3-,* and *EML4-NTRK3*-driven tumors, larotrectinib treatment led to a significantly longer survival compared to treatment with entrectinib. It is unclear whether this effect is related to fusion or tumor biology. In our *in vitro* systems we observed that entrectinib was more potent against *TPM3-NTRK1*-expressing cells compared to *GKAP1-NTRK2*- and *ETV6-NTRK3*-expressing cells. In general, larotrectinib (100 mg/kg) was better tolerated than entrectinib (30 mg/kg) by tumor-bearing mice, limiting the active concentration that could be administered. We observed increased p-ERK levels in tumors of entrectinib-treated mice, suggesting that ERK signaling might contribute to resistance to TKI therapy. *In vitro*, MEK inhibition with trametinib was able to inhibit the growth of NTRK fusion-driven cells, and a combination of TKIs and MEK inhibitors was superior to either treatment alone. *In vivo,* MEK inhibition was able to significantly inhibit the growth of ETV6-N3-driven flank tumors, albeit less effectively than TKIs. This is likely due to compensatory mechanisms by other pathways (such as the PI3K-AKT-mTOR pathway) that are inhibited by TKIs but not by MEKi. These data highlight the importance of the RAF-MEK-ERK pathway in NTRK fusion-positive pediatric gliomas.

In summary, this study highlights the utility of GEMMs of specific oncogenic drivers to optimize therapy of tumors driven by specific molecular mechanisms where clinical trials are not possible because of their rarity. These models will be valuable tools for the study of treatment response and the development of resistance to therapy in these tumors.

Limitations of the study

We acknowledge several limitations inherent to the experimental design of these studies. One is related to the use of mice that harbor a general loss of *Cdkn2a* gene expression in all cells to induce the formation of tumors harboring *Cdkn2a* loss. In future work studying the interactions between tumor cells and the microenvironment, *Cdkn2a* loss can be induced specifically in tumor cells using a $Cdkn2a^{flox/flox}$ line or a short hairpin RNA (shRNA) system. A second limitation was the use of NIH 3T3 cells for the development of an *in vitro* cell model. We confirmed all results with a second cell model derived from primary RCAS mouse tumor cells. However, further studies of the downstream pathways induced by NTRK

fusions using additional cell-line models, such as neural stem cell-based models, could give different results. A third point is that we observed a high percentage of hydrocephalus when expressing NTRK gene fusions in p0–p2 pups, hindering the use of these tumors for preclinical studies. We overcame this issue by expressing the fusions in slightly older mice (p7). However, *Cdkn2a* wild-type tumors induced at p7 were less aggressive and rarely symptomatic, and we therefore had to use tumors harboring *Cdkn2a* loss for preclinical experiments. Finally, it will be important to study the effect of neoadjuvant TKI treatment on the efficacy of surgical tumor resection, and vice versa, to address the question of whether TKI delivery into the surgical cavity may increase intratumoral drug concentration. For practical reasons we did not undertake surgical resection of these experimental gliomas, but future research will be necessary to answer these questions.

RESOURCE AVAILABILITY

Lead contact

Requests for further information and resources and reagents should be directed to and will be fulfilled by the lead contact, Frank Szulzewsky (Frank.Szulzewsky@hsc.utah.edu).

Materials availability

All materials are available from the lead contact upon request.

Data and code availability

- All data reported in the paper are available from the lead contact upon request.
- This paper does not report original code.
- Any additional information required to reanalyze the data reported in this paper is available from the lead contact upon request.

STAR★METHODS

EXPERIMENTAL MODEL AND STUDY PARTICIPANT DETAILS

All animal experiments were done in accordance with protocols approved by the Institutional Animal Care and Use Committees of Fred Hutchinson Cancer Center (protocol no. 50842) and followed National Institutes of Health guidelines for animal welfare. Tumors were induced using the RCAS/tv-a system [19]. *Nestin* (N)/tv-a;*Cdkn2a*-wild type and null mice were used for RCAS-mediated brain tumor formation in this study [19]. DF1 cells (1×10^5) in a volume of 1 μL were injected near the ventricles into newborn (p0-p2) or one-week-old (p7) pup brains or into the striatum of 5-7-week-old adult mice [19,27]. For peripheral injections, DF1 cells (1×10^5) in a volume of 1-2 μL were injected intraperitoneally (i.p.) or subcutaneously. Mice were monitored until they developed symptoms of disease, such as visible tumors, lethargy, poor grooming, weight loss, dehydration, macrocephaly, seizures, jumping, or paralysis, or until a predetermined study end point.

METHOD DETAILS

***In vivo* treatment of mice—**For *in vivo* treatment with TKIs, inhibitors were resuspended in DMSO and diluted to a final buffer solution of 10% DMSO, 10% EtOH, 30% Solutol (Sigma Aldrich 42966), and 50% Tartaric acid buffer. Tartaric acid buffer stock was prepared by mixing 10 ml of 0.15 M DL-tartaric acid (Sigma Aldrich PHR1472) with 50 ml of 0.15 M tartrate sodium (Sigma Aldrich PHR1409). 10 ml of the Tartaric acid buffer stock were subsequently mixed with 40 ml of Saline Solution (0.9%) to create the final Tartaric acid buffer. Mice were treated with either Vehicle (10% DMSO), Larotrectinib (100 mg/kg), or Entrectinib (30 or 60 mg/kg) at 10 ul pergram i.p. injection twice-a-day (b.i.d.) for 14 days.

For *in vivo* treatment with Trametinib, RCAS-ETV6-NTRK3 flank tumors were induced by subcutaneous injection into p7 Nestin/tv-a Cdkn2a null mice. When palpable tumors were observed, mice were treated with either Vehicle (DMSO in corn oil), Trametinib (1 mg/kg), or Entrectinib (15 mg/kg) via oral gavage, once-a-day, 5 days per week (Monday – Friday) and tumor calipers were measured daily (Monday – Friday). Mice were removed from the study once tumors reached a diameter of 20 mm.

Determining TKI doses for *in vivo* treatment—Mice were treated by i.p. injection of drug twice-a-day (b.i.d.). To assess the optimal *in vivo* inhibitor concentrations for treatment, we first treated non-tumor mice with different doses of either Entrectinib (20, 30, 40, 60 mg/kg, two mice per group) or Larotrectinib (46, 92,138 mg/kg, three mice per group) for several days to assess general drug toxicity. One mouse treated with 20 mg/kg Entrectinib died during treatment, while one mouse treated with 92 mg/kg Larotrectinib died two days after the last treatment. In general, we observed that mice treated with either 92 or 138 mg/kg Larotrectinib developed distended abdomens due to fluid retention that receded several days after treatment discontinuation. We first treated several mice with intracranial gliomas with Larotrectinib (60 or 100 mg/kg), Entrectinib (30 or 60 mg/kg), or Vehicle for 7 days and subsequently analyzed the treated tumors by histology. We observed a greater tumor response at 100 mg/kg Larotrectinib compared to 60 mg/kg and no toxicity-related deaths in either cohort. Similarly, we observed a greater response at 60 mg/kg Entrectinib compared to 30 mg/kg, however, observed several toxicity-related deaths at 60 mg/kg. Based on these results, we proceeded with a dosing strategy of 100 mg/kg Larotrectinib and 30 mg/kg Entrectinib.

Quantification of Larotrectinib tissue levels—Mice were treated for 48 hours with 100 mg/kg Larotrectinib b.i.d. (five treatments in total) and intra- and extra-cranial tumor tissue, as well as hindlimb muscle and liver tissue was isolated and flash frozen. A weighed portion of the tissue was homogenized in 20 vol of PBS with a pestle fitted for a micro centrifuge tube. A 20 μL aliquot (1 mg tissue) of the homogenate was used for each analysis. The samples were deproteinized with 4 vol of a solution made of 1:1 Acetonitrile: Methanol containing 0.02 μM D5-Nilotinib as an internal standard. The samples were centrifuged at 10000 g for 8 min, and 5 μl of the supernatant was injected into the LC/MS. Compounds were separated on a C18 column using a gradient mixture of 16 mM Ammonium Formate and 1:1 Acetonitrile: Methanol at a flow rate of 0.25 ml/min. Compounds were identified

by their protonated molecular ions, 429.1850 amu (Larotrectinib) and 536.2293 amu (D5-Nilotinib) with a mass tolerance of 5 ppm, and concurrent fragmentation scans were used to further confirm the identity of the compounds. For quantitation, standard curves were generated by adding known amounts of Larotrectinib to untreated tissue homogenates. Ratios of Larotrectinib peak area to D5-Nilotinib peak area were found to be linear to the added amount of Larotrectinib from 0.004 to 42 ng/mg. The lower limit of quantitation was set at 0.004 ng Larotrectinib/mg tissue.

Plasmid generation—Primers used for plasmid generation are listed in Table S1A. Additional plasmids used in this study are listed in Table S1C.

Transfection of RCAS viruses—Chicken fibroblast (DF1) cells were maintained with 10% fetal bovine serum (FBS) in Dulbecco's modified Eagle medium (DMEM) (including 1% Penicillin/Streptomycin) at 39 degrees Celsius. DF-1 cells were transfected with the indicated RCAS plasmid using X-tremeGENE 9 DNA transfection reagent (Roche) according to the manufacturer's protocol. RCAS transgene expression was confirmed via western blot analysis.

Generation of NTRK fusion-expressing NIH-3T3 cells—Viral supernatant from DF1 cultures was sterile-filtered and added to Tv-a-expressing NIH-3T3 cells [28] every eight hours. NIH-3T3-tv-a cells were maintained with 10% Newborn CALF serum (Thermo Fisher 26010074) in DMEM (including 1% Penicillin/Streptomycin) at 37 degrees Celsius. RCAS transgene expression was confirmed via western blot analysis.

Culturing of primary mouse tumor cells—Primary mouse tumors generated by flank injection of RCAS-producing DF1 cells into Nestin/tv-a Cdkn2a null mice were manually dissected using scalpels and maintained with 10% FBS in DMEM (including 1% Penicillin/Streptomycin) at 37 degrees Celsius. RCAS transgene expression was confirmed via western blot analysis.

Spheroid assay—NIH-3T3-tv-a cells (expressing either GFP, TPM3-NTRK1 (or mutants thereof), GKAP1-NTRK2, or ETV6-NTRK3) or primary mouse tumor cells were seeded at $4x10^3$ cells per well in a 96-well ultra-low attachment plates (Corning 7007) in DMEM with 10% FBS and spun down at 1250 rpm for 10 minutes. After 2 days, cells were treated with DMSO or TKIs at indicated concentrations. Growth of spheroids was monitored using live cell imaging every 24 hours for 5 days in the Incucyte ZOOM system (Essen). Average phase object area (mm^2) was used for analysis. Viability was measured using the CellTiter-Glo® 2.0 Cell Viability Assay (Promega G9241) according to the manufacturer's instructions. Luminescence was detected using a Veritas Microplate Luminometer.

Magnetic resonance imaging (MRI)—Tumor size and progression were evaluated using the preclinical 7 Tesla MR scanner (MR Solutions, DRYMAG7.0T) located in the FHCC imaging suite.

The first MRI was performed 15-25 days post-injection (for exact times see below). Treatment started one day after the MRI. TPM3-NTRK1 (15 days post-injection), CHTOP-

NTRK1 (15 days post-injection); GKAP1-NTRK2 (15 days post-injection); NACC2-NTRK2 (18 days post-injection); ETV6-NTRK3 (25 days post-injection).

Following anesthetic induction with 2% isoflurane, each mouse was placed on a bed and respiration was monitored via pneumatic pillow (SA Instruments, ERT gating module). Mouse body temperature was maintained by warm air circulation within the arm. Each procedure lasted approximately 10-30 minutes. Images were acquired using a mouse brain RF coil. Techniques used are Fast Spin Echo (FSE) T2 weighted scans (FSE T2w (axial) TE=75, 15 slices at 0.5mm thickness, FOV 25, 1 average) and for contrast enhanced imaging FSE T1 weighted scan pre- and post-contrast injection (FSE T1w (axial) TE=11, 15 slices at 0.5mm thickness, FOV 25, 2 averages). For contrast enhanced imaging 1 mL Gadobenate (MultiHance 529mg/ml, 0.5M) was diluted in 9 mL saline and mice were dosed with 4 ul/g of solution. Following imaging, each mouse was allowed to recover from anesthesia in a warm recovery cage. Tumor volumes based on MRI images were calculated using the software 3D slicer and graphed with GraphPad Prism.

H&E staining, immunohistochemistry stainings of FFPE mouse tissues—For routine tumor histomorphology, mouse brains and peripheral tumors were formalin-fixed and paraffin-embedded, sectioned, and stained with H&E [29,30]. For stainings in Figures 2 and S2, mouse brains were cut along the sagittal plane into 4 pieces, flash frozen in liquid nitrogen, and subsequently thawed in formalin and subsequently processed as described above. Immunohistochemical (IHC) staining of mouse brains was performed on the DISCOVERY XT platform (Ventana Medical Systems, Inc., Tucson, U.S.A) using the Discovery DAB Map Detection Kit according to standard protocols [31]. For a list of antibodies used see Table S1B. IHC images were quantified using HistoQuant software.

Western Blot—Cells were cultured, lysed, and processed for western blotting by standard methods. Proteins were resolved by SDS/PAGE (NuPAGE 10% Bis/Tris; LifeTech) according to XCell Sure Lock Mini-Cell guidelines, blocked with 5% milk/TBST and probed with specified antibodies overnight at 4°C in 5% BSA/TBST. After three TBST rinses, species-specific secondary antibodies were added in 5% milk/TBST. Blots were rinsed three times with TBST before being developed with Amersham ECL Western Blotting Detection Reagents (GE Healthcare). For a list of antibodies used see Table S1B.

Quantification of RCAS integrations in RCAS-ETV6-NTRK3 flank tumors—Mouse tumor tissue was flash frozen in liquid nitrogen and genomic DNA was subsequently isolated using the Qiagen DNeasy Blood & Tissue Kit (Cat. 69504). PCR experiments were carried out on a QuantStudio™ 7 Flex Real-Time PCR System. The forward primer was located in the C terminal region of NTRK3 and the reverse primer in the RCAS viral backbone. Mouse Actb primers were used for reference. For primer sequences see Table S1A.

Chemicals—Larotrectinib (LOXO-101, NSC 785570), Entrectinib (NMS-E628, NSC 774769), Repotrectinib (TPX-0005, NSC 800522), and Selitrectinib (LOXO-195, NSC 809970) were provided through the National Institutes of Health (NIH) Developmental

Therapeutics Program. Trametinib (GSK1120212, Cat. S2673), Taselisib (GDC 0032, Cat. S7103), and PLX8394 (Cat. S7965) were purchased from Selleckchem.

QUANTIFICATION AND STATISTICAL ANALYSIS

All statistical analyses were conducted using GraphPad Prism 10 (GraphPad software Inc.). Statistical differences between 2 populations were calculated by unpaired t test (2-tailed). For multiple populations' comparison, one-way or two-way ANOVA with Turkey's multiple-comparisons test was used. $p < 0.05$ was considered statistically significant.

Supplementary Material

Refer to Web version on PubMed Central for supplementary material.

ACKNOWLEDGMENTS

We thank Denis Adair, Linda Lew, and Kelly Grissom for continued administrative assistance and support throughout these experiments. We thank Elizabeth Jensen and Dolores Covarrubias at the Fred Hutchinson Genomics Core for help with DNA sequencing. We thank Brianna Wrightson and Elena Carlson for developing and performing the MRI scans on tumor-bearing mice. Funding for this study was provided by National Institutes of Health grants U54 CA243125 (E.C.H.) and R35 CA253119-01A1 (E.C.H.), Preclinical Imaging Shared Resource RRID:SCR_022616, National Institutes of Health grant P30 CA015704 (Fred Hutch/University of Washington Cancer Consortium), and National Institutes of Health Shared Instrumentation grant S10OD26919 (Fred Hutch/University of Washington Cancer Consortium). This project was funded in part by federal funds from the National Cancer Institute, National Institutes of Health, under Contract no. 75N91019D00024, Task Order no. Q3. The content of this publication does not necessarily reflect the views or policies of the Department of Health and Human Services, nor does mention of trade names, commercial products, or organizations imply endorsement by the US government.

REFERENCES

1. Doz F, van Tilburg CM, Geoerger B, Højgaard M, Øra I, Boni V, Capra M, Chisholm J, Chung HC, DuBois SG, et al. (2022). Efficacy and safety of larotrectinib in TRK fusion-positive primary central nervous system tumors. Neuro Oncol. 24, 997–1007. 10.1093/neuonc/noab274. [PubMed: 34850167]
2. Cocco E, Scaltriti M, and Drilon A (2018). NTRK fusion-positive cancers and TRK inhibitor therapy. Nat. Rev. Clin. Oncol 15, 731–747. 10.1038/s41571-018-0113-0. [PubMed: 30333516]
3. Clarke M, Mackay A, Ismer B, Pickles JC, Tatevossian RG, Newman S, Bale TA, Stoler I, Izquierdo E, Temelso S, et al. (2020). Infant High-Grade Gliomas Comprise Multiple Subgroups Characterized by Novel Targetable Gene Fusions and Favorable Outcomes. Cancer Discov. 10, 942–963. 10.1158/2159-8290.CD-19-1030. [PubMed: 32238360]
4. Guerreiro Stucklin AS, Ryall S, Fukuoka K, Zapotocky M, Lassaletta A, Li C, Bridge T, Kim B, Arnoldo A, Kowalski PE, et al. (2019). Alterations in ALK/ROS1/NTRK/MET drive a group of infantile hemispheric gliomas. Nat. Commun 10, 4343. 10.1038/s41467-019-12187-5. [PubMed: 31554817]
5. Wu G, Diaz AK, Paugh BS, Rankin SL, Ju B, Li Y, Zhu X, Qu C, Chen X, Zhang J, et al. (2014). The genomic landscape of diffuse intrinsic pontine glioma and pediatric non-brainstem high-grade glioma. Nat. Genet 46, 444–450. 10.1038/ng.2938. [PubMed: 24705251]
6. Gambella A, Senetta R, Collemi G, Vallero SG, Monticelli M, Cofano F, Zeppa P, Garbossa D, Pellerino A, Rudà R, et al. (2020). NTRK Fusions in Central Nervous System Tumors: A Rare, but Worthy Target. Int. J. Mol. Sci 21, 753. 10.3390/ijms21030753. [PubMed: 31979374]
7. Drilon A, Laetsch TW, Kummar S, DuBois SG, Lassen UN, Demetri GD, Nathenson M, Doebele RC, Farago AF, Pappo AS, et al. (2018). Efficacy of Larotrectinib in TRK Fusion-Positive Cancers in Adults and Children. N. Engl. J. Med 378, 731–739. 10.1056/NEJMoa1714448. [PubMed: 29466156]

8. Doebele RC, Drilon A, Paz-Ares L, Siena S, Shaw AT, Farago AF, Blakely CM, Seto T, Cho BC, Tosi D, et al. (2020). Entrectinib in patients with advanced or metastatic NTRK fusion-positive solid tumours: integrated analysis of three phase 1-2 trials. Lancet Oncol. 21, 271–282. 10.1016/S1470-2045(19)30691-6. [PubMed: 31838007]

9. Hong DS, DuBois SG, Kummar S, Farago AF, Albert CM, Rohrberg KS, van Tilburg CM, Nagasubramanian R, Berlin JD, Federman N, et al. (2020). Larotrectinib in patients with TRK fusion-positive solid tumours: a pooled analysis of three phase 1/2 clinical trials. Lancet Oncol. 21, 531–540. 10.1016/S1470-2045(19)30856-3. [PubMed: 32105622]

10. Drilon A, Siena S, Ou SHI, Patel M, Ahn MJ, Lee J, Bauer TM, Farago AF, Wheler JJ, Liu SV, et al. (2017). Safety and Antitumor Activity of the Multitargeted Pan-TRK, ROS1, and ALK Inhibitor Entrectinib: Combined Results from Two Phase I Trials (ALKA-372-001 and STARTRK-1). Cancer Discov. 7, 400–409. 10.1158/2159-8290.CD-16-1237. [PubMed: 28183697]

11. Drilon A, Nagasubramanian R, Blake JF, Ku N, Tuch BB, Ebata K, Smith S, Lauriault V, Kolakowski GR, Brandhuber BJ, et al. (2017). A Next-Generation TRK Kinase Inhibitor Overcomes Acquired Resistance to Prior TRK Kinase Inhibition in Patients with TRK Fusion-Positive Solid Tumors. Cancer Discov. 7, 963–972. 10.1158/2159-8290.CD-17-0507. [PubMed: 28578312]

12. Drilon A, Ou SHI, Cho BC, Kim DW, Lee J, Lin JJ, Zhu VW, Ahn MJ, Camidge DR, Nguyen J, et al. (2018). Repotrectinib (TPX-0005) Is a Next-Generation ROS1/TRK/ALK InhibitorThat Potently Inhibits ROS1/TRK/ALK Solvent-Front Mutations. Cancer Discov. 8, 1227–1236. 10.1158/2159-8290.CD-18-0484. [PubMed: 30093503]

13. Cocco E, Schram AM, Kulick A, Misale S, Won HH, Yaeger R, Razavi P, Ptashkin R, Hechtman JF, Toska E, et al. (2019). Resistance to TRK inhibition mediated by convergent MAPK pathway activation. Nat. Med 25, 1422–1427. 10.1038/s41591-019-0542-z. [PubMed: 31406350]

14. Arakaki AKS, Szulzewsky F, Gilbert MR, Gujral TS, and Holland EC (2021). Utilizing preclinical models to develop targeted therapies for rare central nervous system cancers. Neuro Oncol. 23, S4–S15. 10.1093/neuonc/noab183. [PubMed: 34725698]

15. Kanvinde PP, Malla AP, Connolly NP, Szulzewsky F, Anastasiadis P, Ames HM, Kim AJ, Winkles JA, Holland EC, and Woodworth GF (2021). Leveraging the replication-competent avian-like sarcoma virus/tumor virus receptor-A system for modeling human gliomas. Glia 69, 2059–2076. 10.1002/glia.23984. [PubMed: 33638562]

16. Chen Z, Herting CJ, Ross JL, Gabanic B, Puigdelloses Vallcorba M, Szulzewsky F, Wojciechowicz ML, Cimino PJ, Ezhilarasan R, Sulman EP, et al. (2020). Genetic driver mutations introduced in identical cell-of-origin in murine glioblastoma reveal distinct immune landscapes but similar response to checkpoint blockade. Glia 68, 2148–2166. 10.1002/glia.23883. [PubMed: 32639068]

17. Ozawa T, Arora S, Szulzewsky F, Juric-Sekhar G, Miyajima Y, Bolouri H, Yasui Y, Barber J, Kupp R, Dalton J, et al. (2018). A De Novo Mouse Model of C11orf95-RELA Fusion-Driven Ependymoma Identifies Driver Functions in Addition to NF-kappaB. Cell Rep. 23, 3787–3797. 10.1016/j.celrep.2018.04.099. [PubMed: 29949764]

18. Szulzewsky F, Arora S, Arakaki AKS, Sievers P, Almiron Bonnin DA, Paddison PJ, Sahm F, Cimino PJ, Gujral TS, and Holland EC (2022). Both YAP1-MAML2 and constitutively active YAP1 drive the formation of tumors that resemble NF2 mutant meningiomas in mice. Genes Dev. 36, 857–870. 10.1101/gad.349876.122. [PubMed: 36008139]

19. Szulzewsky F, Arora S, Hoellerbauer P, King C, Nathan E, Chan M, Cimino PJ, Ozawa T, Kawauchi D, Pajtler KW, et al. (2020). Comparison of tumor-associated YAP1 fusions identifies a recurrent set of functions critical for oncogenesis. Genes Dev. 34, 1051–1064. 10.1101/gad.338681.120. [PubMed: 32675324]

20. Wang Y, Long P, Wang Y, and Ma W (2020). NTRK Fusions and TRK Inhibitors: Potential Targeted Therapies for Adult Glioblastoma. Front. Oncol 10, 593578. 10.3389/fonc.2020.593578. [PubMed: 33330081]

21. Frattini V, Trifonov V, Chan JM, Castano A, Lia M, Abate F, Keir ST, Ji AX, Zoppoli P, Niola F, et al. (2013). The integrated landscape of driver genomic alterations in glioblastoma. Nat. Genet 45, 1141–1149. 10.1038/ng.2734. [PubMed: 23917401]

22. Leeman-Neill RJ, Kelly LM, Liu P, Brenner AV, Little MP, Bogdanova TI, Evdokimova VN, Hatch M, Zurnadzy LY, Nikiforova MN, et al. (2014). ETV6-NTRK3 is a common chromosomal

rearrangement in radiation-associated thyroid cancer. Cancer 120, 799–807. 10.1002/cncr.28484. [PubMed: 24327398]

23. Komori T (2017). Pathology of oligodendroglia: An overview. Neuropathology 37, 465–474. 10.1111/neup.12389. [PubMed: 28548216]
24. Edmondson R, Broglie JJ, Adcock AF, and Yang L (2014). Three-dimensional cell culture systems and their applications in drug discovery and cell-based biosensors. Assay Drug Dev. Technol 12, 207–218. 10.1089/adt.2014.573. [PubMed: 24831787]
25. Isozaki H, Sakhtemani R, Abbasi A, Nikpour N, Stanzione M, Oh S, Langenbucher A, Monroe S, Su W, Cabanos HF, et al. (2023). Therapy-induced APOBEC3A drives evolution of persistent cancer cells. Nature 620, 393–401. 10.1038/s41586-023-06303-1. [PubMed: 37407818]
26. Tognon CE, Mackereth CD, Somasiri AM, McIntosh LP, and Sorensen PHB (2004). Mutations in the SAM domain of the ETV6-NTRK3 chimeric tyrosine kinase block polymerization and transformation activity. Mol. Cell Biol 24, 4636–4650. 10.1128/MCB.24.11.4636-4650.2004. [PubMed: 15143160]
27. Wirsching HG, Zhang H, Szulzewsky F, Arora S, Grandi P, Cimino PJ, Amankulor N, Campbell JS, McFerrin L, Pattwell SS, et al. (2019). Arming oHSV with ULBP3 drives abscopal immunity in lymphocyte-depleted glioblastoma. JCI Insight 4, e128217. 10.1172/jci.insight.128217. [PubMed: 31292299]
28. Ozawa T, Riester M, Cheng YK, Huse JT, Squatrito M, Helmy K, Charles N, Michor F, and Holland EC (2014). Most human non-GCIMP glioblastoma subtypes evolve from a common proneural-like precursor glioma. Cancer Cell 26, 288–300. 10.1016/j.ccr.2014.06.005. [PubMed: 25117714]
29. Holland EC, Celestino J, Dai C, Schaefer L, Sawaya RE, and Fuller GN (2000). Combined activation of Ras and Akt in neural progenitors induces glioblastoma formation in mice. Nat. Genet 25, 55–57. 10.1038/75596. [PubMed: 10802656]
30. Hambardzumyan D, Amankulor NM, Helmy KY, Becher OJ, and Holland EC (2009). Modeling Adult Gliomas Using RCAS/t-va Technology. Transl. Oncol 2, 89–95. 10.1593/tlo.09100. [PubMed: 19412424]
31. Herting CJ, Chen Z, Pitter KL, Szulzewsky F, Kaffes I, Kaluzova M, Park JC, Cimino PJ, Brennan C, Wang B, and Hambardzumyan D (2017). Genetic driver mutations define the expression signature and microenvironmental composition of high-grade gliomas. Glia 65, 1914–1926. 10.1002/glia.23203. [PubMed: 28836293]

Highlights

- Both N-terminal fusion partner and NTRK variant influence tumor aggressiveness and biology
- Tyrosine kinase inhibition prolongs survival, but persister cells lead to recurrence
- Resistance-associated point mutations influence response to therapy *in vivo*
- MEK inhibition leads to a significant growth inhibition *in vivo*

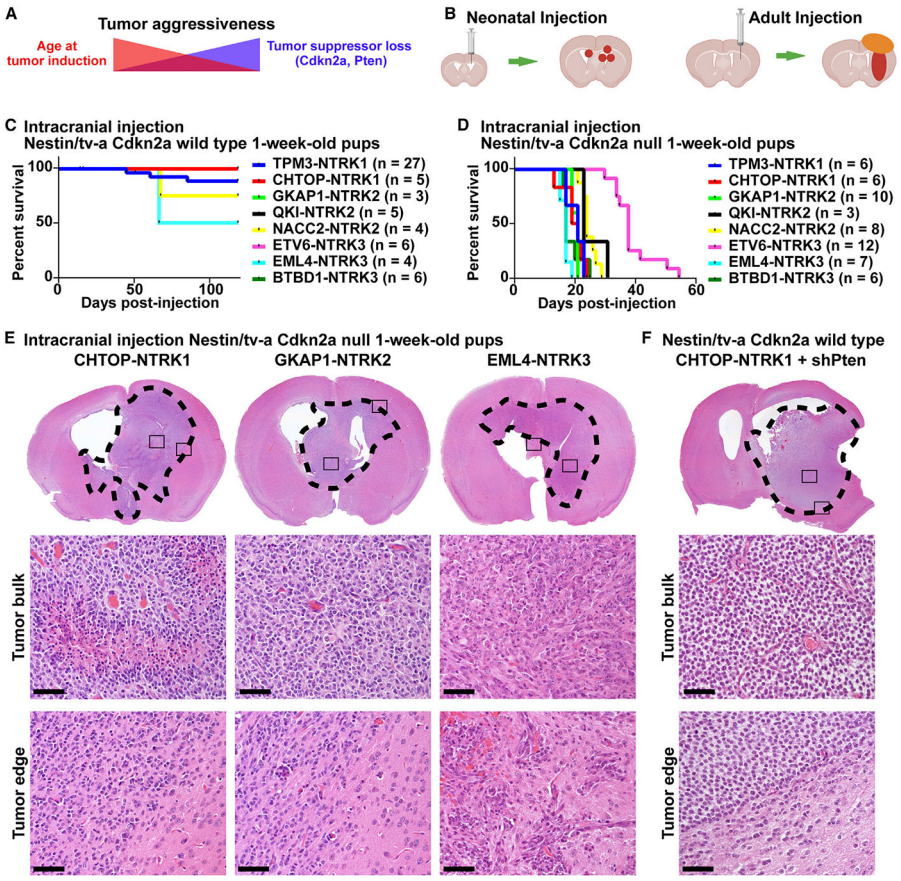

Figure 1. Expression of *NTRK* gene fusions in Nestin-positive cells induces the formation of experimental mouse gliomas

(A) Influence of age at time of tumor induction and loss of additional tumor suppressors on tumor aggressiveness.

(B) Schematic depicting RCAS injection and tumor formation for neonatal and adult mice.

(C) Symptom-free survival of Nestin/tv-a (N/tv-a) *Cdkn2a* wild-type mice upon intracranial expression of *NTRK* gene fusions.

(D) Symptom-free survival of N/tv-a *Cdkn2a* null mice upon intracranial expression of different *NTRK* gene fusions.

(E) H&E staining of mouse gliomas induced by expression of *CHTOP-NTRK1*, *GKAP1-NTRK2,* or *EML4-NTRK3* in 1-week-old N/tv-a *Cdkn2a* null mice.

(F) H&E staining of a mouse glioma induced by expression of *CHTOP-NTRK1* in 1-week-old N/tv-a *Cdkn2a* wild-type mice with additional knockdown of *Pten*.

Scale bars indicate 50 μm. Black dotted lines indicate tumor boundaries (E and F). See also Figure S1.

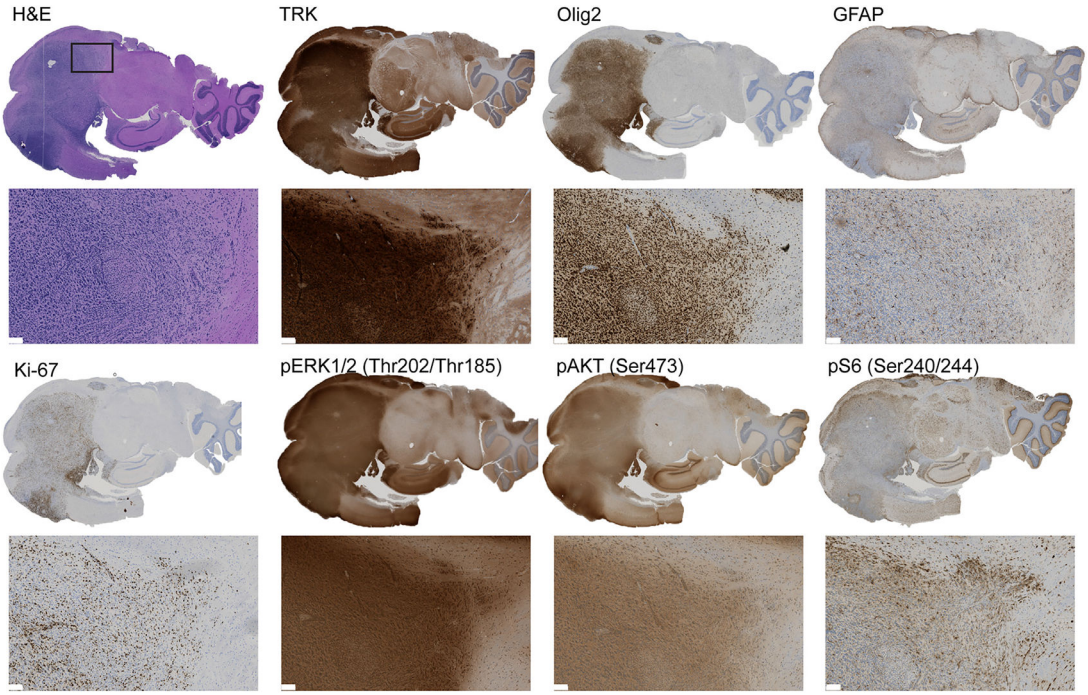

Figure 2. *NTRK* fusion-driven experimental mouse gliomas show activation of the PI3K-AKT-S6 and RAF-MEK-ERK pathways

Representative IHC staining of a *TPM3-NTRK1*-driven mouse glioma for TRK (TRK kinase domain), Olig2, GFAP, Ki-67, phospho-ERK1/2 (Thr202/Thr185), phospho-AKT (Ser473), and phospho-S6 (Ser240/244). Scale bars indicate 100 μm. See also Figure S2.

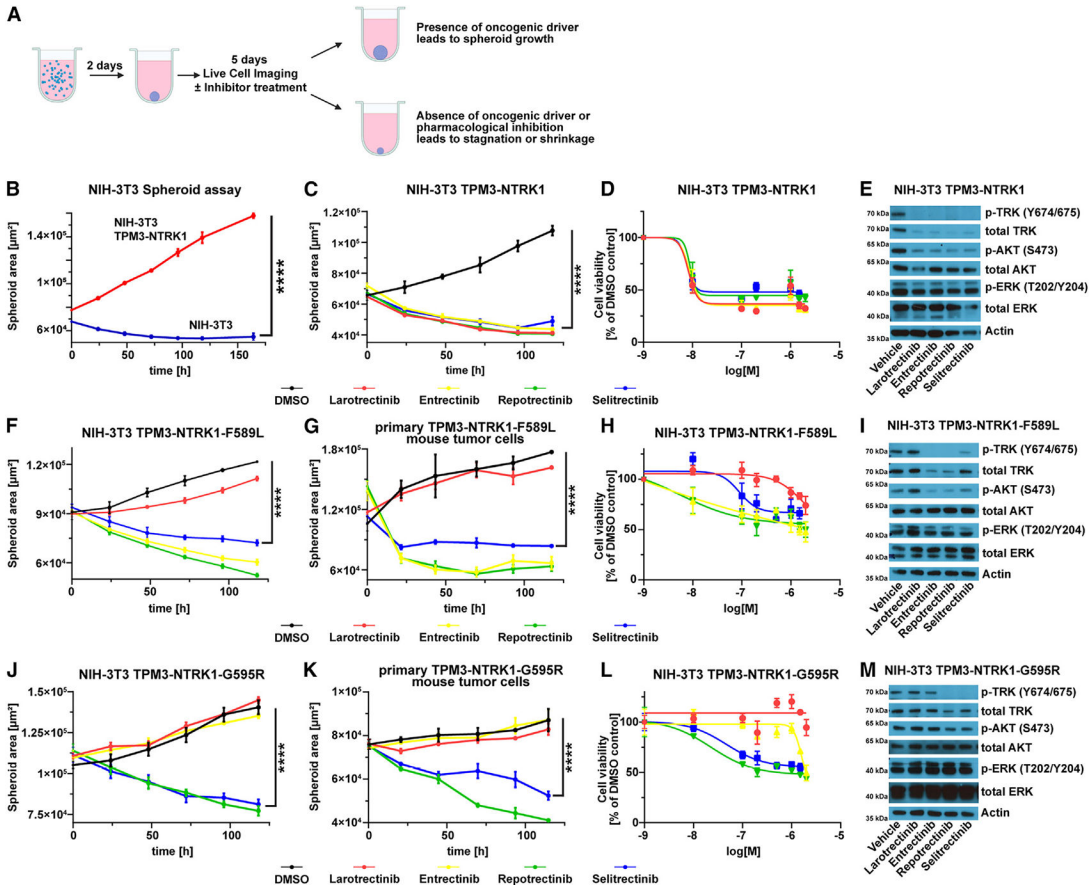

Figure 3. Resistance-associated kinase domain point mutations influence the response of *NTRK* fusion-driven cells to TKI treatment *in vitro*

(A) Schematic overview of 3D spheroid assay.

(B) Growth curve of a 3D spheroid assay with either untransduced NIH-3T3-tv-a cells (blue line) or cells expressing *TPM3-NTRK1* (red line) ($n = 3$).

(C) Growth curve of TPM3-NTRK1-expressing NIH-3T3-tv-a cell spheroids treated with either DMSO (0.1%) or the indicated TKIs (100 nM each) ($n = 3$).

(D) Dose-response curve of TPM3-NTRK1-expressing NIH-3T3-tv-a cell spheroids treated with different TKI concentrations relative to DMSO-treated cells ($n = 3$).

(E) Western blot of TPM3-NTRK1-expressing NIH-3T3-tv-a cells treated with the indicated TKIs at 100 nM.

(F and G) Growth curves of TPM3-NTRK1-F589L-expressing NIH-3T3-tv-a (F) or primary mouse tumor (G) cell spheroids treated with either DMSO (0.1%) or the indicated TKIs (100 nM each) ($n = 3$).

(H) Dose-response curve of TPM3-NTRK1-F589L-expressing NIH-3T3-tv-a cell spheroids treated with different TKI concentrations relative to DMSO-treated cells ($n = 3$).

(I) Western blot of TPM3-NTRK1-F589L-expressing NIH-3T3-tv-a cells treated with the indicated TKIs at 100 nM.

(J and K) Growth curves of TPM3-NTRK1-G595R-expressing NIH-3T3-tv-a (J) or primary mouse tumor (K) cell spheroids treated with either DMSO (0.1%) or the indicated TKIs (100 nM each) ($n = 3$).

(L) Dose-response curve of TPM3-NTRK1-G595R-expressing NIH-3T3-tv-a cell spheroids treated with different TKI concentrations (same as D) relative to DMSO-treated cells ($n = 3$).
(M) Western blot of TPM3-NTRK1-G595R-expressing NIH-3T3-tv-a cells treated with the indicated TKIs at 100 nM.
Error bars show SEM. Analysis was done using ordinary two-way ANOVA (B, C, F, G, J, and K). **** $p < 0.0001$. See also Figure S3.

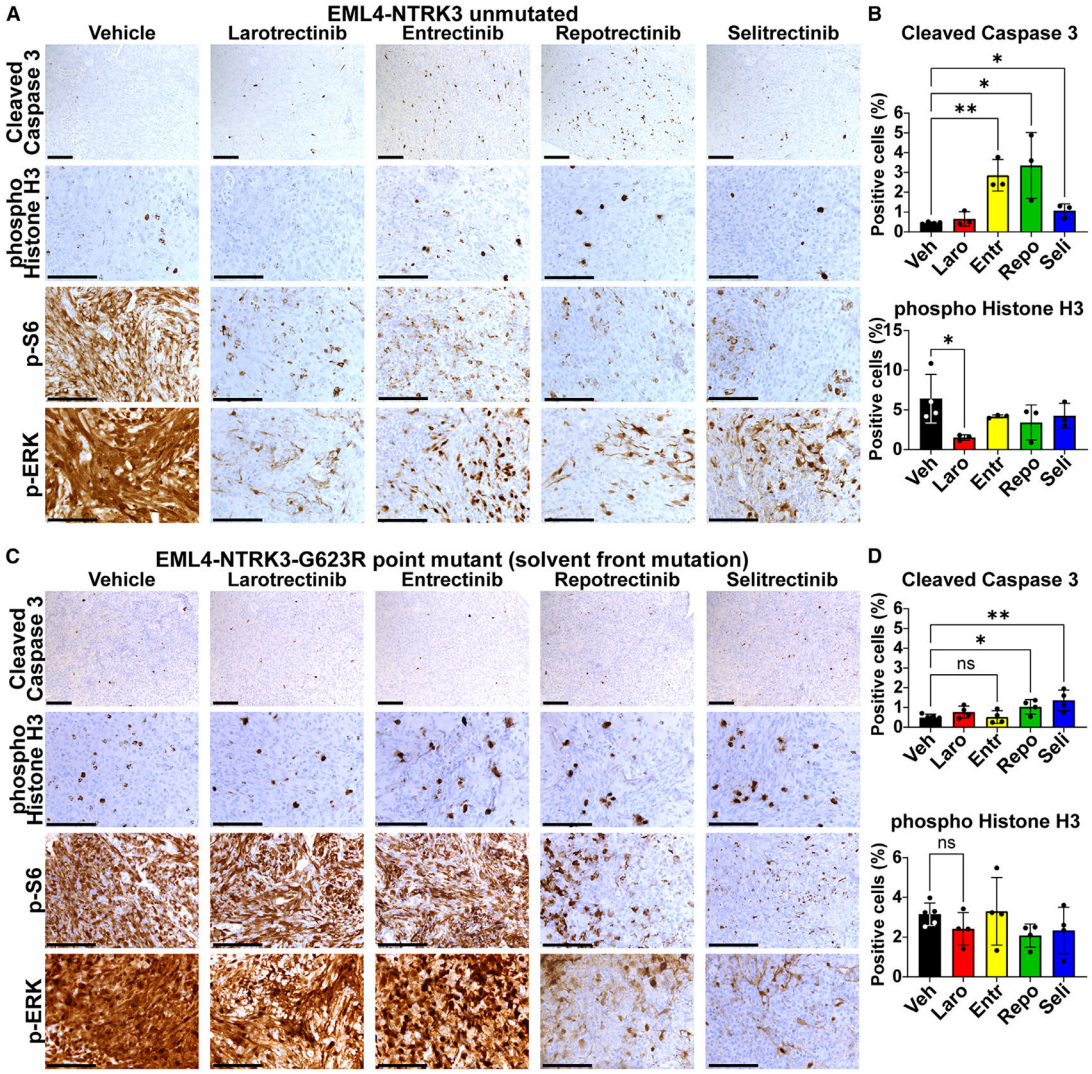

Figure 4. Resistance-associated kinase domain point mutations influence the response of *NTRK* fusion-driven cells to TKI treatment *in vivo*

(A) IHC staining of EML4-NTRK3-driven mouse gliomas treated *in vivo* with either vehicle or larotrectinib (100 mg/kg), entrectinib (60 mg/kg), repotrectinib (20 mg/kg), or selitrectinib (20 mg/kg) for 25 h.

(B) Quantification of CC3 and pHH3 staining of EML4-NTRK3-driven mouse gliomas treated with either vehicle or the four different TKIs ($n = 4$ for vehicle, $n = 3$ for the different TKIs).

(C) IHC staining of EML4-NTRK3-G623R-driven mouse gliomas treated with either vehicle or TKIs (same as A) for 25 h.

(D) Quantification of CC3 and pHH3 staining of EML4-NTRK3-G623R-driven mouse gliomas treated with either vehicle or the four different TKIs ($n = 5$ for vehicle, $n = 4$ for the different TKIs).

Scale bars indicate 100 μm. Error bars show SD. Analysis was done using two-tailed t test (B). *$p < 0.05$, **$p < 0.01$. See also Figure S4.

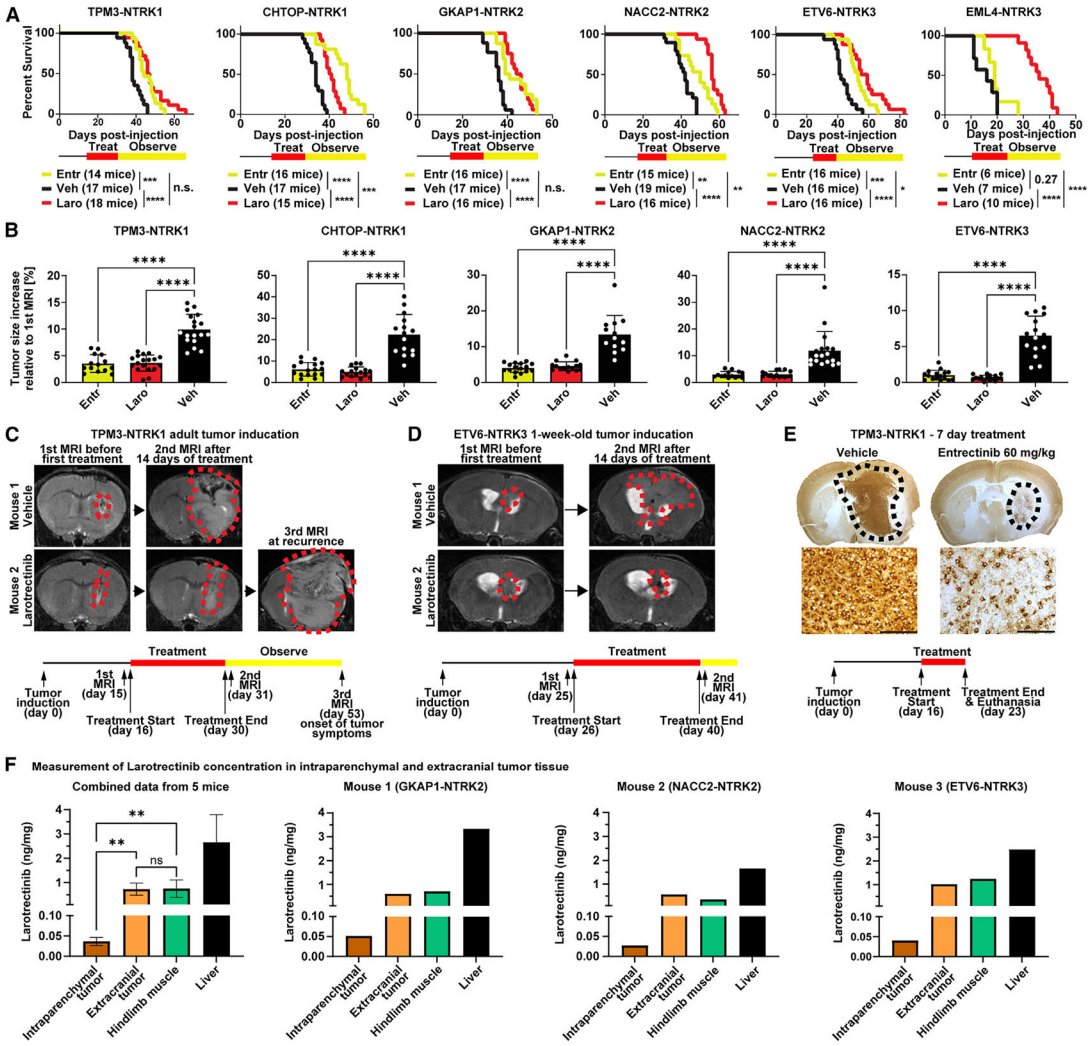

Figure 5. TKI treatment significantly prolongs the survival of NTRK gene fusion-driven mouse gliomas

(A) Symptom-free survival of mice harboring *TPM3-NTRK1-, CHTOP-NTRK1-, GKAP1-NTRK2-, NACC2-NTRK2-, ETV6-NTRK3-,* and *EML4-NTRK3*-driven gliomas treated with vehicle, larotrectinib (100 mg/kg), or entrectinib (30 mg/kg) via intraperitoneal (i.p.) injection twice a day (b.i.d.) for 14 days. After treatment discontinuation, the mice were observed for the onset of tumor-related symptoms.

(B) Change in tumor size during the 14-day period of treatment with vehicle, larotrectinib, or entrectinib as measured by MRI.

(C and D) MRIs of mice harboring *TPM3-NTRK1* (C)- or *ETV6-NTRK3* (D)-driven tumors treated with either vehicle or larotrectinib.

(E) IHC staining (TRK kinase domain) of *TPM3-NTRK1* mouse gliomas after 7 days of treatment (i.p.; b.i.d.) with either vehicle or entrectinib (60 mg/kg).

(F) Larotrectinib concentration in intraparenchymal tumor ($n = 5$), extracranial tumor ($n = 3$), hindlimb muscle ($n = 5$), or liver tissue ($n = 5$) taken from mice treated with larotrectinib (100 mg/kg) via i.p. injection b.i.d. for 48 h (five treatments total). Red or black dotted lines indicate tumor boundaries. Scale bars indicate 100 μm.

Error bars show SD. Analysis was done using log-rank (Mantel-Cox) test (A) or ordinary one-way ANOVA (B and F). *$p < 0.05$, **$p < 0.01$, ***$p < 0.001$, and ****$p < 0.0001$. See also Figure S5.

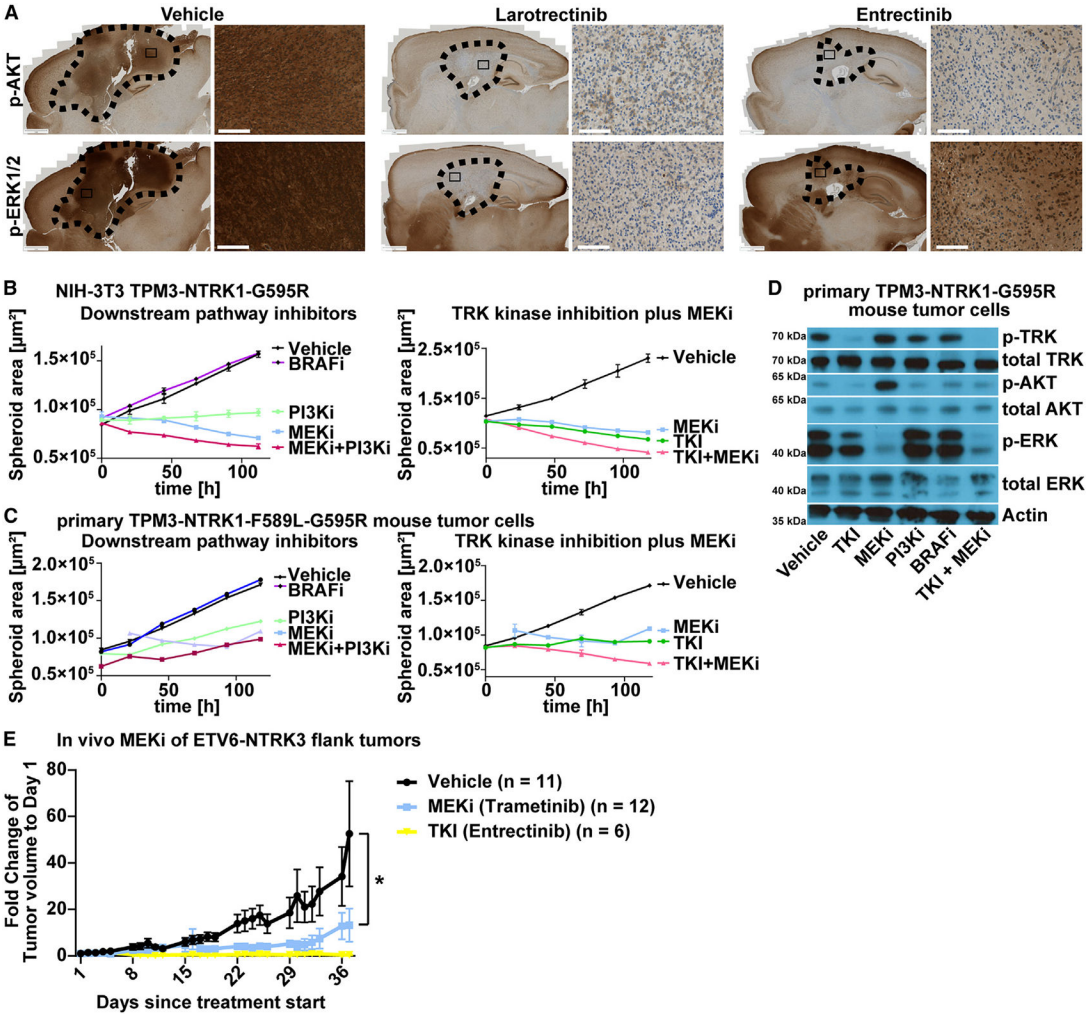

Figure 6. Combination therapy of TRK and MEK inhibition is superior to TRK inhibition alone against NTRK fusion-driven cells

(A) IHC staining of *ETV6-NTRK3* mouse gliomas (vehicle or 14 days of larotrectinib [100 mg/kg] or entrectinib [30 mg/kg] treatment). Black dotted lines indicate tumor boundaries. Scale bars indicate 1 mm (whole-brain slides) or 100 µm (high-magnification images).

(B and C) Growth curves of TPM3-NTRK1-G595R-expressing NIH-3T3-tv-a (B) or primary TPM3-NTRK1-F589L-G595R mouse tumor (C) cell spheroids treated with DMSO (0.1%), repotrectinib (TKI), trametinib (MEKi), taselisib (PI3Ki), PLX8394 (BRAFi), or a combination of repotrectinib plus trametinib (TKI + MEKi) ($n = 3$). All inhibitors were used at 100 nM except for trametinib at 10 nM.

(D) Representative Western blot of primary TPM3-NTRK1-G595R mouse tumor cells treated with either DMSO (0.1%; vehicle) or the indicated inhibitors (same as in C and D).

(E) *In vivo* treatment of ETV6-NTRK3-driven flank tumors with vehicle, trametinib (1 mg/kg), or entrectinib (15 mg/kg). Graph shows fold change in tumor volume compared to day 1 of treatment.

Error bars show SEM. Analysis was done using ordinary two-way ANOVA (E). *$p < 0.05$. See also Figure S6.

KEY RESOURCES TABLE

REAGENT or RESOURCE	SOURCE	IDENTIFIER
Antibodies		
HA (IHC)	Cell Signaling	3724; RRID:AB_1549585
GFAP	Dako	Z0334; RRID:AB_10013382
phospho-Histone H3 (Ser10)	Upstate	06-570; RRID:AB_310177
total TRK	abcam	ab76291; RRID:AB_1524514
Olig2	Cell Signaling	65915; RRID:AB_2936997
Olig2	Millipore	AB9610; RRID:AB_570666
Ki67	Cell Signaling	12202; RRID:AB_2620142
Cleaved Caspase-3 (Asp175)	Cell Signaling	9661; RRID:AB_2341188
Phospho-S6 Ribosomal Protein (Ser240/244)	Cell Signaling	5364; RRID:AB_10694233
Phospho-S6 Ribosomal Protein (Ser235/236)	Cell Signaling	4858; RRID:AB_916156
phospho-AKT (S473)	abcam	ab81283; RRID:AB_2224551
ERK1 (phospho T202) + ERK2 (phospho T185)	abcam	ab214036; RRID:AB_2923008
phospho-ERK (Thr202/Tyr204)	Cell Signaling	4370; RRID:AB_2315112
Biotinylated Goat Anti-Rabbit IgG Antibody	Vector	BA-1000; RRID:AB_2313606
HA (IF)	Roche	11867423001; RRID:AB_390918
donkey anti-rat 488	Invitrogen	A-21208; RRID:AB_141709
donkey anti-rabbit Cy3	Jackson Immuno	711-165-152; RRID:AB_2307443
Actin	Sigma	A1978; RRID:AB_476692
ECL Mouse IgG, HRP-linked	GE Healthcare	NA931; RRID:AB_772210
ECL Rabbit IgG, HRP-linked	GE Healthcare	NA934; RRID:AB_772206
phospho-TRK (Tyr674/675) (Western Blot)	Cell Signaling	4621; RRID:AB_916186
phospho-AKT (S473) (Western Blot)	Cell Signaling	4060; RRID:AB_2315049
total AKT	Cell Signaling	9272; RRID:AB_329827
total ERK	Cell Signaling	9102; RRID:AB_330744
Bacterial and virus strains		
Stellar™ Competent Cells	Takara Bio	636763
RCAS (Replication-Competent ASLV long terminal repeat (LTR) with a Splice acceptor)	This lab	N/A
Biological samples		
Mouse tumor tissue	This lab	N/A
Chemicals, peptides, and recombinant proteins		
X-tremeGENE 9 DNA transfection reagent	Roche	XTG9-RO
Newborn CALF serum	Thermo Fisher	26010074
Larotrectinib	National Institutes of Health (NIH) Developmental Therapeutics Program	LOXO-101, NSC 785570
Entrectinib	National Institutes of Health (NIH) Developmental Therapeutics Program	NMS-E628, NSC 774769
Repotrectinib	National Institutes of Health (NIH) Developmental Therapeutics Program	TPX-0005, NSC 800522

REAGENT or RESOURCE	SOURCE	IDENTIFIER
Selitrectinib	National Institutes of Health (NIH) Developmental Therapeutics Program	LOXO-195, NSC 809970
Trametinib (GSK1120212)	Selleckchem	S2673
Taselisib (GDC 0032)	Selleckchem	S7103
PLX8394	Selleckchem	S7965
Solutol	Sigma Aldrich	42966
DL-tartaric acid	Sigma Aldrich	PHR1472
tartrate sodium	Sigma Aldrich	PHR1409
MultiHance® (gadobenate dimeglumine)	Bracco	N/A
Critical commercial assays		
CellTiter-Glo® 2.0	Promega	G9241
Experimental models: Cell lines		
DF1 cells	ATCC	CRL-3586
NIH-3T3	ATCC	CRL-1658
NIH-3T3-tv-a	This lab	N/A
Experimental models: Organisms/strains		
Nestin (N)/tv-a	This lab	N/A
Nestin (N)/tv-a; Cdkn2a −/−, Pten flox/flox	This lab	N/A
Oligonucleotides		
See Table S1A		
Recombinant DNA		
See Table S1C		
Software and algorithms		
ImageJ		RRID:SCR_003070
Prism 10	GraphPad	RRID:SCR_002798
3D slicer		RRID:SCR_005619
Other		
96-well ultra-low attachment plates	Corning	7007